Journal of Controlled Release 384 (2025) 113947

Contents lists available at ScienceDirect

Journal of Controlled Release

journal homepage: www.elsevier.com/locate/jconrel

A biodegradable suction patch for sustainable transbuccal peptide delivery

Hanna Krupke [a], Nicole Zoratto [a], Lucie Rabut [a], Daniel Gao [a], Nevena Paunović [a], David Klein Cerrejon [a], Benoit Dehapiot [b], Jean-Christophe Leroux [a,*]

[a] Institute of Pharmaceutical Sciences, Department of Chemistry and Applied Biosciences, ETH Zurich, 8093 Zurich, Switzerland
[b] Scientific Center for Optical and Electron Microscopy (ScopeM), ETH Zurich, 8093 Zurich, Switzerland

ARTICLE INFO

Keywords:
Biodegradable polymers
Peptide delivery
Buccal patch
Permeation enhancement

ABSTRACT

Despite considerable advances in the systemic delivery of peptides, their susceptibility to gastrointestinal degradation and high molecular weight, which restricts permeability across biological barriers, remain obstacles to oral administration. As a result, most peptide therapies rely on injections to achieve therapeutic effects. Recent studies on a bioinspired suction patch demonstrated positive effects *in vivo* with three peptides – desmopressin, semaglutide, and teriparatide – yet materials used for patch fabrication were non-degradable. In this work, a more sustainable patch alternative is introduced by replacing previously used materials with biodegradable polymers, aiming for degradation of the patch after removal to reduce environmental impact. A scalable mold casting process was employed to thermally crosslink synthesized and functionalized copolyesters, yielding the desired devices. Mechanical testing across various materials and shapes identified the best-performing polymer, while its degradation was confirmed in both aqueous medium and simulated waste. An *ex vivo* model using porcine buccal tissue validated the functionality of biodegradable patches, showing enhanced permeation of a poorly permeable dye when combined with a chemical permeation enhancer. In beagle dogs, the bioavailability of semaglutide (4.11 kDa) was substantially improved compared to the commercially available tablet, with an application time of only 10 min. Additionally, the patch achieved a relative bioavailability of 26% for bremelanotide (1.03 kDa) compared to subcutaneous administration. This work underscores the potential of replacing silicone devices with biodegradable alternatives, providing a more sustainable approach for peptide delivery *via* the buccal suction patch.

1. Introduction

Peptide drugs are effective treatment options across a wide range of diseases [1,2]. However, due to their physicochemical properties, most of these drugs are applied as injectables – especially when their molecular weight (MW) exceeds 1 kDa [3]. Despite over a century of research, parenteral injections remain the common method for delivering peptide drugs and other macromolecular therapeutics due to their effectiveness in providing high plasma levels; yet their invasive nature and associated discomfort can negatively impact patients' quality of life and treatment acceptance [4,5]. Moreover, parenteral dosing requires syringes, and improper separation of the different waste types they produce – such as glass, sharps, and biohazardous materials – negatively affects the environment [6].

While the oral route is preferred by both patients and healthcare professionals, the gastrointestinal (GI) tract presents a hostile environment for many macromolecules due to low pH and proteolytic enzymes that degrade them [7]. Only a small fraction of peptides can surmount these breakdown processes, while their high MW further limits their ability to efficiently traverse the GI epithelial barrier [8]. Consequently, only a few oral dosage forms containing peptides with MW > 1 kDa have received Food and Drug Administration (FDA) approval by leveraging specific features of the peptides or formulations. The cyclic and lipophilic peptide cyclosporine A and its derivative voclosporine exhibit unusually high membrane permeability due to their conformational flexibility [9], while desmopressin compensates for its low oral bioavailability with substantial potency and a large therapeutic index [10]. On the other hand, the oral delivery of semaglutide (SMG) is in part enabled by its long half-life ($t_{1/2}$, 7 days [11]) and coformulation with high amounts of the chemical permeation enhancer (PE) salcaprozate sodium (SNAC) (*i.e.*, 300 mg per tablet). SNAC is claimed to promote gastric absorption of the drug partially by locally

* Corresponding author.
E-mail address: jleroux@ethz.ch (J.-C. Leroux).

https://doi.org/10.1016/j.jconrel.2025.113947
Received 3 April 2025; Received in revised form 3 June 2025; Accepted 9 June 2025
Available online 11 June 2025

raising the pH, thereby protecting it against enzymatic degradation [12]. Similarly, sodium caprylate serves as a key component in the Transient Permeation Enhancer (TPE®) technology, which is used in Mycapssa®, an oily suspension formulation designed to promote the oral delivery of octreotide [13]. While attempts at combining, for example, SNAC with other peptidic drugs showed beneficial effects [14], successful translation from research to a broader range of clinical applications has yet to be realized.

Besides chemical PEs [15,16], other strategies aimed at enhancing macromolecular GI absorption are being investigated, including proximity-based devices [17,18] and physical methods like jet- [19] and (micro)needle-based injections [20–25]. While some of these systems incorporate biodegradable components [19] or are designed to be completely degraded in the body [17,24], many still rely on non-degradable materials. For example, in the case of GI injectors, applied steel springs or plastic balloons increase the environmental burden, while their manufacturing complexity and intricate delivery mode make the achieved bioavailability often highly variable.

Other routes for systemic macromolecule delivery face distinct challenges that limit their applications: rapid clearance after pulmonary inhalation [26,27], high variability associated with intranasal delivery [28,29], and production challenges of transdermal systems [30]. Furthermore, these dosage forms contain non-degradable components, and, in the case of inhalation therapy, contribute to plastic waste from inhalers [31].

The buccal route offers several advantages for non-invasive drug delivery, including ease of administration, mild pH relative to other parts of the GI tract, high blood flow, and avoidance of the hepatic first-pass effect [32–36]. However, transbuccal permeation is relatively ineffective for macromolecules [37], and even though slight increases in permeation have been reported with mucoadhesive systems and/or nanoparticles [38–40] as well as PEs [41,42], FDA-approved buccal products are still limited to small molecules [43]. Consequently, device-based strategies – such as microneedle systems [44,45] or jet injectors

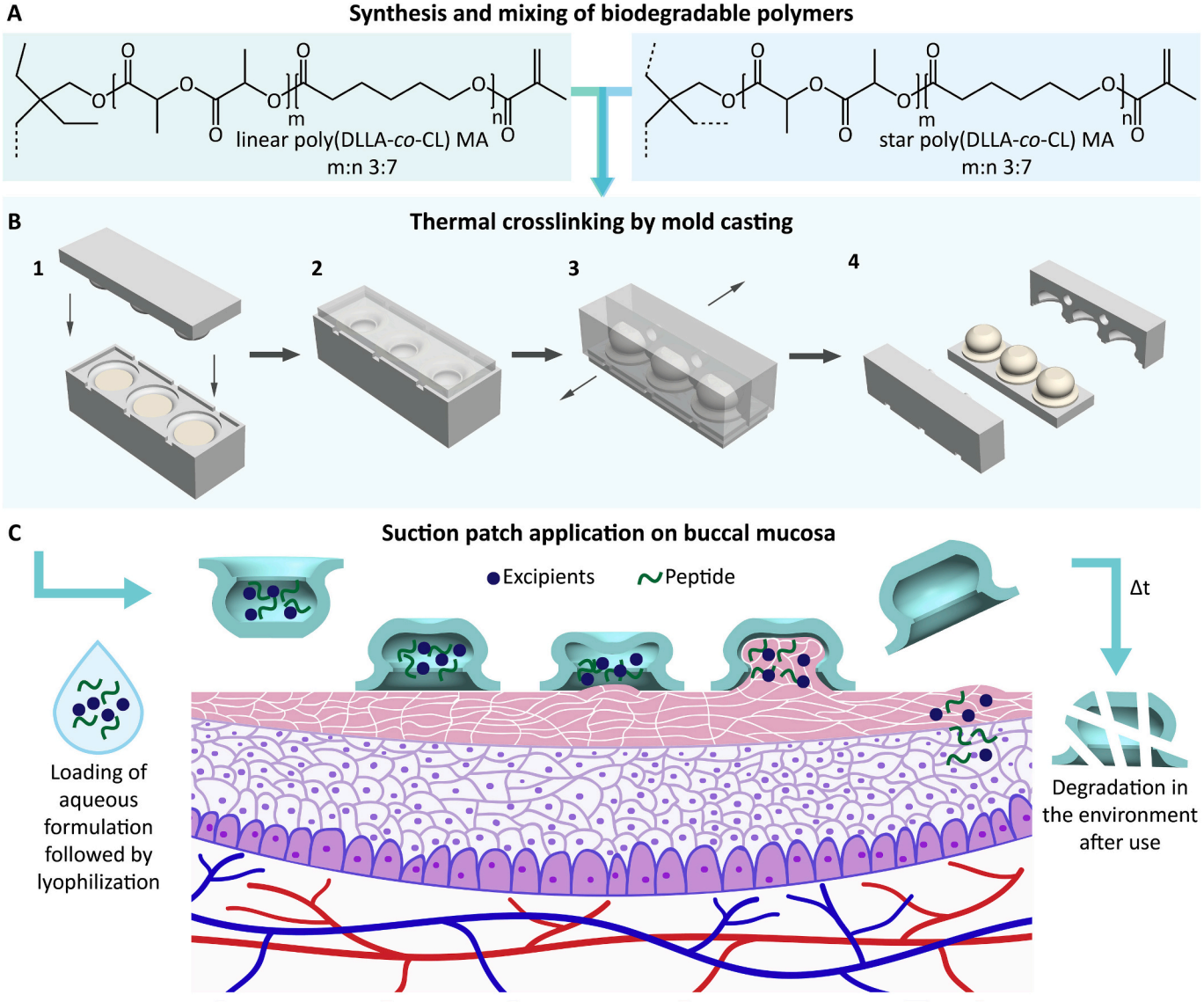

Fig. 1. Concept of the biodegradable suction cup orifice design (SCOD). A) Synthesis and functionalization of linear and star-shaped poly(DL-lactide-*co*-ε-caprolactone) (poly(DLLA-*co*-CL)) yield methacrylated poly(DLLA-*co*-CL) (poly(DLLA-*co*-CL) MA). B) Thermal crosslinking of poly(DLLA-*co*-CL) MA in molds enables SCOD formation *via* a scalable process (1: Resin filling, 2: Stamp insertion, 3: Crosslinking, 4: Mold opening and demolding). C) Once loaded with the peptide formulation, the patch is applied to the buccal mucosa by manual compression. Releasing this compressive force generates hypobaric pressure, causing a suction effect that establishes contact between the tissue and the formulation. After application, the patch can be removed and disposed of, followed by degradation of the patch material over time in the environment.

like the MucoJet [46] – have become a key focus in ongoing efforts to improve the delivery of macromolecules through the buccal mucosa [47]. Our group recently reported the suction cup orifice design (SCOD), a flexible buccal device that integrates PEs with a mechanical stretching element to increase drug permeation across the buccal mucosa. Conceptualized as a platform technology, the reported SCOD made from non-degradable polymers with strong, elastic properties demonstrated effectiveness with desmopressin, SMG, and teriparatide [48,49]. To enable the developed technology to fulfill its industrial potential, it is becoming increasingly important to replace non-degradable components with environmentally friendly alternatives. This is especially important for devices intended for frequent use in chronic diseases, as the non-hazardous, degradable medical waste would be a more convenient alternative to the complex disposal of syringes commonly used for most macromolecules.

Here, we describe a low-waste version of the SCOD with scalable manufacturing by mold casting of biodegradable polymers (Fig. 1), responding to the call for more sustainable solutions in the pharmaceutical field. As conventional biodegradable polymers used in device formulations are predominantly characterized by low elasticity and high stiffness [50], we chose to synthesize tailorable copolymers of poly(D,L-lactide-*co*-ε-caprolactone) (poly(DLLA-*co*-CL)), followed by functionalization yielding poly(DLLA-*co*-CL) methacrylate (poly(DLLA-*co*-CL) MA) [51,52] which were then thermally crosslinked into the desired device shape. The optimal combination of material and design geometry, integrating the targeted biodegradability feature with the original prototype's functionality, was identified through mechanical testing, degradation experiments, and *ex vivo* performance evaluation. This low-waste SCOD was then loaded with bremelanotide (BMT) (1.03 kDa) or SMG (4.11 kDa), and the pharmacokinetic (PK) profiles of the peptides were determined in beagle dogs after transbuccal delivery.

2. Materials and methods

2.1. Materials

Tablets for preparation of phosphate-buffered saline (PBS) (1 tablet in 200 mL of water yields 10 mM phosphate buffer, 2.7 mM potassium chloride and 137 mM sodium chloride (NaCl)), methanol-free paraformaldehyde (PFA), bovine serum albumin (≥ 98%) (BSA), azobisisobutyronitrile (> 98%) (AIBN), dichloromethane (99+%) (DCM), 2,2-diethyl-1,3-propanediol (99%), 3,6-dimethyl-1,4-dioxane-2,5-dione (99%) (DLLA), 2-methylbutane (≥ 99%), dimethyl sulfoxide-d_6 (DMSO-d_6), 2-propanol (≥ 99.8%, for cleaning), methacryloyl chloride (97%), poly(vinyl alcohol) (PVA) 9–10 k, sodium bicarbonate ($NaHCO_3$), NaCl, tin(II) 2-ethylhexanoate (*ca.* 95%) ($Sn(Oct)_2$), tetrahydrofuran (> 99.5%, high-performance liquid chromatography (HPLC) grade) (THF), Triton™ X-100, (+)-α-tocopherol (vitamin E), N-vinylpyrrolidone (≥ 99%) (NVP), microcrystalline cellulose (MCC), octyl-β-D-glucopyranoside (> 98%) (OGP), tris(hydroxymethyl)aminomethane (≥ 99.9%) (Trizma® base, Tris) and cis-diltiazem hydrochloride (> 99%) were purchased from Sigma Aldrich. PBS (pH 7.4, 1.059 mM potassium phosphate monobasic, 155 mM NaCl, 2.966 mM sodium phosphate dibasic), antibiotic-antimycotic 100× (10′000 units of penicillin, 10 mg of streptomycin, and 25 μg of amphotericin B per mL), acetonitrile (Optima™ grade) (ACN), ammonium hydroxide (28%) (NH_4OH), formic acid (ACS grade) (FA), methanol (Optima™ grade) (MeOH), Dulbecco's modified Eagle's medium with nutrient mixture F-12 (DMEM/F-12, without phenol red), and sterile water for injections (WFI) were bought from Thermo Fisher Scientific. Sodium decanoate (> 99%) (C10) and ε-caprolactone (> 99%) (CL) were obtained from Tokyo Chemical Industry. ProLong™ Diamond Antifade Mountant and Hoechst 33342 dye were bought from Invitrogen. Triethylamine (> 99%) (Et_3N) and ethanol absolute (> 99.8%) (EtOH) were purchased from Merck Millipore. Taurocholic acid sodium salt (≥ 98%) (NaTaC), celite (Celite® Hyflo Super Cel®), and corn seed oil (Ph. Eur., refined) were obtained from Roth AG. Hydrochloric acid (37%) (HCl) and urea (> 99.5%) were purchased from VWR. Sodium sulfate anhydrous (≥ 99%) (Na_2SO_4) and 2-propanol (Optima™ grade, for HPLC) were purchased from Fisher Scientific. Pentaerythritol (98%) was obtained from Acros Organics. Phalloidin-iFluor 488 reagent (ab176753) was purchased from Abcam. Optimal cutting medium (OCT) was obtained from Biosystems. Sulfocyanine 5 free carboxylic acid (Cy5) was bought from Lumiprobe. Silpuran® 6000/50 A and B parts (poly(dimethylsiloxane) (PDMS) Shore A (ShA) hardness 50) were obtained from Wacker Chemie AG. Silicagel (2–5 mm) was obtained from Hänseler AG. Liraglutide (> 95%) was bought from Toronto Research Chemicals. SMG-Na salt (≥ 98%) was purchased from Career Henan Chemical. BMT (≥ 98%, containing 80 m % mannitol as lyoprotectant) was obtained from UK Peptides, or as BMT acetate hydrate from Toronto Chemicals (> 95%). Glycerol (pure, Pharma grade) was purchased from PanReac Applichem. ShA 00 PDMS was obtained from Silikonfabrik. Saccharose (granulated sugar) and corn starch (Maizena) were bought from Coop. Sawdust (from beech wood, 0.1–1 mm corn size) was obtained from MycoGenetics Pilz-Shop. Rabbit feed (MultiFit, Alfalfa) was bought from Fressnapf (MultiFit Tiernahrung). Ripe compost (Quality mature compost) was purchased from Caìscio Compost Sagl. All materials were used as received.

2.2. Polymer synthesis

Poly(DLLA-*co*-CL)s were synthesized by ring-opening polymerization (ROP) using $Sn(Oct)_2$ as a catalyst and with 2,2-diethyl-1,3-propanediol and pentaerythritol as initiators for linear (P1) and star-shaped (P2) polymers, respectively (Fig. S1) [51,52]. For both P1 and P2, the molar feed ratios of DLLA:CL were 3:7. Polymers were further functionalized in DCM using methacryloyl chloride in the presence of Et_3N. Conversions of monomers, as well as methacrylation degree, were analyzed by ^1H nuclear magnetic resonance (NMR) spectroscopy (Figs. S2 and S3). The dispersity (*Đ*) was determined by size exclusion chromatography (SEC) (Fig. S4, Table S1).

For the synthesis of P1, 2,2-diethyl-1,3-propanediol (0.37 g, 2.8 mmol), DLLA (14.62 g, 101 mmol), CL (27 g, 237 mmol), and $Sn(Oct)_2$ (8.4 μL, 0.026 mmol) were added to a 100-mL Schlenk flask. The flask was placed under vacuum for 1.5 h and purged with argon before repeating this cycle twice with 30 min of vacuum to remove oxygen and water. The reaction was performed in an oil bath at 140 °C for 24 h under stirring (400 rpm). Conversions of DLLA and CL were 96–98% and 97–99%, respectively, and number average molecular weights ($M_{n\ NMR}$) of 14′550–14′800 g/mol were obtained by ^1H NMR spectroscopy (Fig. S2). Representative SEC analysis revealed a *Đ* of 1.64 and a $M_{n\ SEC}$ of 18′490 g/mol (Fig. S4A, Table S1). The crude polymer was then dissolved in 150 mL DCM, and after adding Et_3N (3 mL, 21.6 mmol), the mixture was purged with nitrogen for *ca.* 15 min. While cooling the mixture on ice, methacryloyl chloride (2 mL, 20.5 mmol) prediluted in 8 mL DCM was added slowly while stirring (600 rpm), and the reaction continued for 24 h. Afterward, the obtained poly(DLLA-*co*-CL) MA was washed with HCl (1 M), $NaHCO_3$ (5 and 8%), and NaCl (saturated) aqueous solutions and dried with anhydrous Na_2SO_4 after addition of vitamin E (*ca.* 0.03 g). The product was filtered through celite, and the organic solvent was evaporated before drying under high vacuum (3–7 days, *ca.* 36 g). ^1H NMR spectroscopy confirmed the conversion of hydroxyl end groups (*ca.* 97%) (Fig. S2), while representative SEC analysis revealed *Đ* and $M_{n\ SEC}$ of 1.71 and 18′190 g/mol, respectively (Fig. S4A, Table S1).

For the synthesis of P2, pentaerythritol (0.38 g, 2.8 mmol), DLLA (14.53 g, 101 mmol), CL (27 g, 238 mmol), and $Sn(Oct)_2$ (8.4 μL, 0.026 mmol) were added to a 100-mL Schlenk flask. The polymerization was then carried out as described for P1, with conversions of 95–97% for DLLA and 98–99% for CL, and an $M_{n\ NMR}$ of 14′600–14′700 g/mol (Fig. S3). The *Đ* and $M_{n\ SEC}$ were 1.43 and 16′880 g/mol, respectively (Fig. S4B, Table S1). The functionalization was performed according to the protocol for P1, yielding a highly viscous polymer (*ca.* 31 g). The end

group conversion of P2-poly(DLLA-*co*-CL) MA was *ca.* 95% (Fig. S3), while the $Đ$ and $M_{n\ SEC}$ were 1.40 and 19′220 g/mol, respectively (Fig. S4B, Table S1).

2.3. Polymer characterization

^{1}H NMR spectra of crude and functionalized poly(DLLA-*co*-CL) were recorded on Bruker AV400 spectrometer (Bruker Corporation) at 400 Hz with DMSO-d_6 as a solvent. The conversions (%) of both DLLA and CL were calculated after polymerization as indicated in eqs. (1) and (2), where A corresponds to the peak area in the ^{1}H NMR spectrum.

$$DLLA_{\%} = \frac{A_{5.2\ ppm}}{A_{5.2\ ppm} + A_{5.4\ ppm}} \times 100 \quad (1)$$

$$CL_{\%} = \frac{A_{2.3\ ppm}}{A_{2.3\ ppm} + A_{2.7\ ppm}} \times 100 \quad (2)$$

Subsequently, the $M_{n\ NMR}$ of crude polymers was determined with eq. (3), with N representing the initial number of equivalents of monomers.

$$M_{n\ NMR} = MW_{initiator} + \frac{N_{DLLA} \times DLLA_{\%}}{100} \times MW_{DLLA} + \frac{N_{CL} \times CL_{\%}}{100} \times MW_{CL} \quad (3)$$

SEC was carried out on an Agilent 1260 Infinity II system with two Shodex columns (GPC LF-804, styrene-divinylbenzene copolymer, Resonac) and a differential refractive index (dRI) detector (Optilab). Polymer samples were dissolved in THF, filtered through 0.2-μm membrane filters (Chromafil®, Macherey-Nagel), and eluted with THF at a flow rate of 1 mL/min. $Đ$ and $M_{n\ SEC}$ were calculated relative to a poly(styrene) standard curve with MWs of 580, 2970, 4490, 10′680, 30′230, 170′800, and 1′820′000 g/mol. Differential scanning calorimetry (DSC) was performed on a TA Q200 DSC (TA Instruments-Waters LLC). Polymers or crosslinked samples (5–10 mg) were placed in Tzero hermetic pans (TA Instruments-Waters LLC) and subjected to heat-cool-heat cycles ranging from −80 to 100 °C at 10 °C/min with constant nitrogen flow (50 mL/min). TA Instruments Universal Analysis 2000 Software (5.5.3) was used to analyze the data obtained. Glass transition temperatures (T_gs) were determined from the second heating cycle. Fourier-transform infrared (FTIR) spectroscopy was carried out on PerkinElmer Spectrum 2 with the software Perkin-Elmer Spectrum (Perkin-Elmer Inc.) in transmission mode from 450 to 4000 cm^{-1}. Viscosity measurements of the resins were conducted using HAAKE RheoStress 600 rotational rheometer (Thermo Electron Corporation) with a cone-plate geometry (35 mm/2°) at a constant temperature of 60 °C and with varying shear rate. Data were analyzed using RheoWin Data Manager (Thermo Electron Corporation).

2.4. Patch design and mold manufacturing

SCOD devices were designed in SolidWorks (Dassault Systèmes SE). SCOD and SCOD L designs were reproduced from previously published data [48,49], whereas a slightly thicker version (SCOD T) was created by increasing the overall top wall thickness (from 1.4 mm for the SCOD L to 1.55 mm for SCOD T) while keeping the same height (6.5 mm). A larger version of the SCOD L (SCOD XL) was designed by increasing the wall thickness and height to 1.55 and 6.65 mm, respectively. Additionally, the bases of both SCOD T and XL were expanded to a total radius of 7 mm (6.5 mm for SCOD L), while the distance between the widest inner and thinnest outer radii (point of minimal wall thickness) was increased from 0.1 (SCOD L) to 0.2 mm (SCOD T and XL). To enable mold casting of the devices, the designs were inverted to negative casting molds. Allowing for simultaneous production of multiple items, three negative device structures were linearly aligned per mold. The molds consisted of three parts each, with two mold halves and one stamp for insertion (Fig. S5). The parts were converted to .stl files and uploaded into the Asiga Composer Software (Asiga). 3D printing was carried out with the digital light processing (DLP) printer Asiga PICO 2 (Asiga) using Formlabs HighTemp V2 resin (Formlabs) with 0.05 mm layer thickness and exposure times of 2 and 0.8 s for the initial and following layers, respectively. After, all parts were cleaned by sonication in 2-propanol for 5 min in a sonicator bath (Ultrasonic cleaner, Labmaterial or Bandelin Sonorex, Bandelin electronic) before subjecting them to additional ultraviolet (UV) curing for 2 h in a UV chamber (CL-1000 Ultraviolet Crosslinker, UVP). For the production of PDMS SCOD L patches, identically designed molds with six linearly aligned device structures were milled from aluminum.

2.5. Thermal crosslinking of synthesized polymers

Resins for thermal crosslinking were prepared by adding *ca.* 5–10 g of poly(DLLA-*co*-CL) MA (P1:P2 mass ratios of 100:0, 80:20, and 60:40) to amber glass vials. AIBN (0.5 m%) and vitamin E (0.25 m%) were dissolved in NVP (NVP:polymer 15:85 m/m), and the mixture was added to the polymer. The resin was then sonicated (Ultrasonic cleaner or Bandelin Sonorex) at *ca.* 60 °C for 15–20 min and manually mixed until a homogenous mixture was obtained. After transferring to molds that were pretreated with mold release agent (Ease Release™ 200, Mann Release Technologies™), degassing was done under vacuum at *ca.* 60 °C for 30 min in a vacuum oven (KVTS 11, Salvis). After insertion of the stamp, all parts were clamped together tightly, allowing crosslinking to proceed for 3 h at 100 °C (KVTS 11). Finally, structures were demolded, excess material was removed with a scalpel, and the crosslinked objects were cleaned by sonication (Ultrasonic cleaner or Bandelin Sonorex) in 2-propanol for 5 min and dried under ambient conditions before use.

2.6. Mold casting of PDMS

PDMS patches were prepared by first mixing the prepolymer components A and B of Silpuran® 6000/50 (ShA 50 hardness) in a 1:1 mass ratio. The mixture was then transferred to a 50-mL centrifuge tube (TPP Techno Plastic Products), centrifuged at 4000 ×*g* for 5 min (Heraeus Megafuge 16, Thermo Scientific), and filled into aluminum molds coated with mold release agent (Ease Release™ 200). Degassing was done for 1 h at room temperature (RT) in a vacuum oven (KVTS 11). Then, the stamp was inserted, all parts were clamped together tightly, and solidification occurred at 100 °C for 5 h in an oven (Memmert). Subsequently, after demolding, excess material was removed, and the patches were tempered for an additional 5 h at 100 °C. The patches were then cleaned by immersion in EtOH for 5 min and dried under ambient conditions before use.

2.7. Tensile testing

To test the mechanical properties of mold-cast specimens, tensile tests were performed on dogbone-shaped test strips (35 × 6 × 1 mm, L_0 = 12 mm) using a texture analyzer with a 50-N load cell (TA.XTplus, Stable Micro Systems). Molds with three strips per mold were designed in SolidWorks and 3D printed as described in Section 2.4. The strips made of poly(DLLA-*co*-CL) MA at P1:P2 of 100:0, 80:20, and 60:40 (m/m), as described in Section 2.5, were pulled at a rate of 6 mm/min until breakage and force-displacement curves were recorded using the Exponent software (Stable Micro Systems). The Young's modulus was calculated as the slope of the stress-strain curve from 0.325% to 0.925% strain. Five strips of each material were tested (n = 5).

2.8. In vitro degradation study

Degradable SCODs were prepared and cleaned as described in Section 2.5, dried under vacuum at RT, weighed (m_0), and placed separately in centrifuge tubes (TPP Techno Plastic Products) containing 50 mL PBS (pH 7.4) at 50 °C with orbital rotation (KS250 basic, IKA Labortechnik). At each time point, SCODs were removed from the buffer, cleaned with deionized (DI) water, dabbed with wipes, and weighed (m_{wet}). After

drying for 24 h under vacuum at RT, SCODs were weighed again (m_{dry}) before placing them in fresh medium.

The remaining mass (%) and water uptake (%) were calculated according to eqs. (4) and (5), respectively.

$$Mass = \frac{m_{dry}}{m_0} \times 100 \quad (4)$$

$$Water\ uptake = \frac{m_{wet} - m_{dry}}{m_{dry}} \times 100 \quad (5)$$

In addition, the pH of the buffer was measured at each time point using a pH electrode (Mettler Toledo) on Irion Dual Star pH/ISE Meter (Thermo Fisher Scientific) at RT. Further, images were taken to visually follow the degradation process over time. The study was performed with four SCODs of each material (n = 4).

2.9. Compression testing

The compressive resistance of different patch designs and materials was assessed with a texture analyzer with a 50-N load cell (TA.XTplus). A custom-designed platform was created in SolidWorks and 3D printed with a commercial resin (Value Line UV/DLP Tough, PrimaCreator) using a liquid-crystal display printer (Jenny Light 1+). After cleaning the platform in 2-propanol by sonication (Ultrasonic cleaner or Bandelin Sonorex) for 5 min and curing in the UV chamber for 2 h (CL-1000 Ultraviolet Crosslinker), a hole with a 2-mm diameter was drilled in a central position to facilitate air release during the compression measurement. After calibrating the instrument height, devices were positioned on the platform and compressed at a rate of 5 mm/s until a force of 50 N was reached (Fig. S6). The Exponent software was used to record force-displacement curves. Measurements were performed in at least four independent experiments (n = 4–6).

2.10. Negative pressure measurement

To determine the negative pressure generated by the devices' application, an in-house pressure setup was used. A customized platform was designed in SolidWorks, 3D printed, and cleaned as described for the platform in Section 2.9. A silicone layer (*ca.* 4-mm thickness) was cast from ShA 00 PDMS [53,54] by mixing parts A and B at 1:1 (m/m), followed by solidification at RT. This thin layer was placed on top of the platform to mimic the mechanical properties of the buccal mucosa. Afterward, a hole with a diameter of 1 mm was drilled through both the PDMS layer and the platform to attach a pressure sensor (Adafruit MPRLS Ported Pressure Sensor Breakout, Adafruit Industries) by sealing the connection with a silicone tube. The sensor was then connected to a Raspberry Pi microcontroller (Raspberry Pi 4 Computer, Model 4 GB RAM, Raspberry Pi Foundation) to enable real-time pressure measurements (Fig. S7). Subsequently, devices were manually compressed onto the silicone layer, and upon release of the compressive force, the pressure was recorded for 10 min. The ambient pressure used for calculating the devices' resulting negative pressure was determined by averaging five consecutive values after patch removal. Measurements were conducted in at least four independent experiments (n = 4–6).

2.11. Adhesion testing

Adhesive properties of the devices were evaluated by measuring their detachment force using the TA.XTplus texture analyzer with a 50-N load cell. To perform this experiment, the patches were extended by a small cylinder at the top of the designs, enabling the insertion of a needle that could be connected to the instrument's upper clamp with a thread (Fig. S8A). For vertical adhesion on silicone, ShA 00 PDMS was mold-cast by mixing parts A and B at a ratio of 1:1 (m/m) and solidifying at RT within a mold that was designed in SolidWorks and 3D printed (Asiga PICO 2) with a commercially available resin (Formlabs Grey Pro, Formlabs). For angled adhesion of devices on ShA 00 PDMS, a platform was designed and 3D printed as described in Section 2.9 (Fig. S8B), and a thin ShA 00 PDMS layer was glued onto the platform before use. The platform or test surface was attached to the lower clamp of the texture analyzer, and after manual compression of the devices onto the substrates, a pulling force was applied at a rate of 5 mm/s until detachment (Fig. S8C). The Exponent software was used to record the force-distance curves. Measurements were performed three times for three to four devices each (n = 3–4).

2.12. Disintegration in synthetic waste

The disintegration of crosslinked poly(DLLA-*co*-CL) MA was assessed in simulated composting conditions following ISO 20200:2015. Sheets (25 × 25 × 1 mm) composed of P1-resin were thermally crosslinked and cleaned as described in Section 2.5. Their mass was recorded after drying under vacuum at 40 °C (KVTS 11) to constant mass (m_i). After, they were shortly immersed in DI water and incubated at 58 °C in polypropylene boxes (33 × 19 × 11 cm, Rotho®) with two holes (5-mm diameter) containing the premixed synthetic waste that was prepared according to ISO 20200:2015 (ratio sample mass to waste mass 0.96–1.04%). The temperature in the oven was continuously monitored using a TM26 temperature indicator (Extech Instruments). At allotted time points, boxes were weighed, and fresh water was added to restore the mass (to 100 or 80% of the original mass), and the compost was mixed, according to the schedule outlined in ISO 20200:2015. Images were taken to visually follow the degradation process over time. After 60 days of incubation, boxes were removed, the mixtures were dried at 58 °C after removing the lids, and clumps were broken apart carefully without damaging the samples. Subsequently, the mixtures were sieved using 10-mm, 5-mm (both Siebmeister 5000, Sterico), and 2-mm (de Buyer) sieves consecutively, followed by visual inspection of residual material not passing the sieves. Fragments that appeared to be leftover samples were pooled and dried under vacuum at 40 °C (KVTS 11) to constant mass. The residual mass of the samples was measured (m_r) to calculate the degree of disintegration (%) (D) with eq. (6).

$$D = \frac{m_i - m_r}{m_i} \times 100 \quad (6)$$

The experiment was performed with six sheets (n = 6).

2.13. Tissue preparation for ex vivo experiments

Porcine buccal tissue from animals *ca.* five to six months of age and with a weight of 85 to 95 kg was obtained freshly from a slaughterhouse in Zurich (Schlachtbetrieb Zürich AG). The fresh tissue was stored in DMEM/F-12 medium (without phenol red) containing 1% (v/v) antibiotic-antimycotic 100× and placed on ice until further processing. Buccal tissue pieces were trimmed within 2 h to remove the outside cheek skin and fat and sectioned into pieces with dimensions of *ca.* 2 × 2 × 2 cm. Pieces with damaged mucosa were excluded, while pieces with visually intact mucosal surfaces were placed in a 6-well plate (TPP Techno Plastic Products), covered with fresh DMEM/F-12 containing 1% (v/v) antibiotic-antimycotic 100×, and incubated at 37 °C (Binder GmbH) for *ca.* 30 min before patch application.

2.14. Suction patch loading and ex vivo application on porcine buccal mucosa

To evaluate the deformation and drug surrogate permeation enhancement upon suction patch application, patches were applied *ex vivo* on freshly excised porcine buccal mucosa. Different patch designs made of P1 (SCOD L, T, and XL) (Section 2.5) were compared with SCOD L made of PDMS (Section 2.6). For patch loading, NaTaC (0 or 3 mg/cup), PVA (0.4 mg/cup), and Cy5 (54 μg/cup) were dissolved in DI water, with a final volume of 100 μL added to each cup. Then, the

formulations were frozen over liquid nitrogen, followed by lyophilization (Alpha 2–4 LSC basic, Christ, Martin Christ Gefriertrocknungsanlagen GmbH) for 4 h before storage in the dark. The patches were then manually compressed onto the porcine buccal mucosa pieces that were prepared as described in Section 2.13, and after removal of spilled dye with PBS, samples were covered with fresh DMEM/F-12 medium (without phenol red) containing 1% (v/v) antibiotic-antimycotic 100× and placed back in the incubator at 37 °C (Binder GmbH) for 30 min. Subsequently, the tissue pieces with attached patches were frozen in an isopentane bath over liquid nitrogen to preserve the deformation. Patches were then peeled off before fully freezing the tissue specimens and embedding them in OCT. All samples were stored at −20 °C until further processing. At least four patches per condition were applied *ex vivo* (n = 4–7).

2.15. Cryosectioning, staining, and imaging of ex vivo samples

Cryosectioning of frozen tissue samples was carried out with a cryostat (CryoStar NX50, Thermo Fisher Scientific). The temperature was set to −20 °C, while the specimens were sectioned at a slice thickness of 20 µm for collection onto adhesive microscopy slides (SuperFrost Plus™, Epredia™). Sections were subsequently fixed with 4% PFA (m/v) in PBS for 5 min, followed by washing in PBS for 3 min. Samples for penetration depth (d_p) quantification were then directly mounted with ProLong™ Diamond Antifade Mountant. For the analysis of the stretching efficiency (*SE*), different sections of each sample were used. First, permeabilization with 5% Triton™ X-100 in 2% (m/v) BSA solution in PBS was done for 15 min, followed by washing for 3 min in PBS. Then, samples were stained by incubation for 30 min in 1% (v/v) phalloidin-iFluor 488 reagent and 1% (v/v) Hoechst in 1% (m/v) BSA solution in PBS, followed by washing in PBS for 3 min and mounting with ProLong™ Diamond Antifade Mountant. Images for d_p quantification were recorded with a Leica DMI 6000 B microscope and light source (EL6000 mercury metal halide bulb, Leica Microsystems) with adaptive focus control at a magnification of ×20 (HC PL FLUOTAR L 20×, with correction collar, numerical aperture: 0.4, dry, Leica Microsystems) using LAS X Software (Leica Microsystems). The tile scan mode (10% tile overlap) was used with manual and automatic focusing, followed by merging to generate final images. Fluorescent light was detected by a monochrome DFC365 FX digital camera (12 bits, 1 × 1 BIN, Leica Microsystems). The Y5 channel (excitation (EX): 590–650 nm, dichroic mirror (DC): 660 nm, emission (EM): 662–738 nm) was used at an exposure time of 150 ms and gain of 5 for all samples. For stained samples, the same system was used as described for d_p samples but with the L5 channel (used for manual and automatic focusing) for phalloidin-iFluor 488 reagent (EX: 460–500 nm, DC: 505 nm, EM: 512–542 nm) at an exposure time of 10–50 ms and gain of 5, and the DAPI channel for Hoechst (EX: 327–383 nm, DC: 400 nm, EM: 435–485 nm) at an exposure time of 3–5 ms and gain of 3.

2.16. Quantification of d_p

The analysis of d_p samples was conducted in Python (version 3.10) using a custom deep learning model for automated tissue detection. The model was trained on 22 binary-annotated images and follows a U-Net architecture with a ResNet18 encoder. It was implemented using the Segmentation Models library [55], which is built on Keras and TensorFlow. The masks generated by the deep learning model were used to identify the surface pixels of the tissue and manually refined to focus on the region of interest (deformed tissue). A Euclidean distance transform was then applied to measure the distance of each tissue pixel from the surface. This distance map (Fig. S9) was used to extract fluorescence intensity profiles relative to tissue depth, with a maximum depth of 5000 µm and bin sizes of 10 µm. All code and training images are available on GitHub [56]. To determine the maximum d_p, the distance values of each sample were first adapted so that the maximal fluorescence intensity (corresponding to the tissue surface) was at 0 µm. The background was determined in ImageJ [57] (version 1.54f) by placing a square (3000 × 3000 pixels) next to the deformation within the tissue and averaging the obtained gray value. This background was subtracted from each value, and the data were normalized to the maximal fluorescence intensity. The reported d_p corresponds to the last intensity value of the normalized data that is above 0.025. Additionally, to visualize the distribution of fluorescence intensity signal, the cumulative area under the curve (*cAUC*) was calculated within different distance segments (negative values after normalization set to 0) and compared to the *cAUC* from 0 to 3000 µm ($cAUC_{0–3000}$). The Excel analysis template for maximum d_p analysis can be found in the raw data.

2.17. Determination of SE

ImageJ [57] (version 1.54f) was used to analyze the tissue surface area in contact with the inside of the patch upon *ex vivo* application. In brief, the L5 channel was used on stained samples (Section 2.15) to determine the tissue outline (Fig. S10A and B) by setting a manual threshold. A line was placed at the bottom of the deformation to separate the deformation from the rest of the tissue (Fig. S10C). The xy-coordinates of the resulting area of deformation were exported, followed by filtering for every 1st in 200 consecutive values to smooth the surface and facilitate further processing. The coordinate set was imported and the points were connected using an open-source macro [58] with slight modifications (Table S2). Then, a spline fit was manually applied in SolidWorks (Fig. S10D). The area was split along a centerline placed perpendicular to the baseline to enable 180° rotation around the centerline of the two generated half-parts (Fig. S10E and F). The total surface area (SA_{total}, mm^2) was determined by summing both half-surfaces, while the final surface area (SA_{final}, mm^2) was calculated by subtracting the ground area (SA_{ground}, mm^2) from SA_{total}, according to eq. (7). SA_{ground} was defined as the measured surface area at each sample's orifice, as derived from the baseline measurement. The *SE* (%) was then determined as the ratio of SA_{final} to the surface area of the internal compartment (SA_{max}, mm^2) of the SCOD design, according to eq. (8). The SA_{max} corresponds to 180 mm^2 for SCOD L and SCOD XL, and 179 mm^2 for SCOD T. Accordingly, a *SE* of 100% indicates complete occupation of the patch's inner compartment by tissue.

$$SA_{final} = SA_{total} - SA_{ground} \tag{7}$$

$$SE = \frac{SA_{final}}{SA_{max}} \times 100 \tag{8}$$

2.18. Preparation of formulations for in vivo studies

SCOD XL patches made of P1 (prepared according to Section 2.5) were used for peptide *in vivo* studies, whereas SCOD L patches made of PDMS (prepared according to Section 2.6) were used as controls for SMG studies. For SMG, 100 µL of DI water containing 2 mg SMG-Na salt, 3 mg NaTaC, and 0.4 mg PVA were loaded into each patch. For BMT patches, 100 µL of DI water containing 2 mg BMT (with *ca.* 8 mg mannitol for 10-min application (UK Peptides), without mannitol for the 20-min application (Toronto Chemicals)) and 3 mg C10 were loaded into each patch. The patches were then frozen over liquid nitrogen and lyophilized for 4 h before being stored in 15-mL centrifugation tubes (TPP Techno Plastic Products) containing silica gel until application. For oral delivery of BMT, size 0 enteric capsules (Capsugel® Enprotect®, Lonza) with a dose of 2 mg BMT (UK Peptides, with mannitol) were prepared by mixing with 250 mg C10 or 250 mg MCC per capsule. A subcutaneous (sc) formulation of BMT was prepared by dissolving BMT (Toronto Chemicals, without mannitol) in WFI containing 2.5% (m/v) glycerol at a concentration of 1.05 mg/mL. The aqueous solution of BMT was then sterile-filtered (0.22 µm, Merck) into an autoclaved glass vial, which was sealed for shipment.

2.19. General protocol and ethical approval for in vivo studies in beagle dogs

All *in vivo* studies were carried out at the Institut national de la recherche scientifique (INRS, CNBE, Laval, Canada). The INRS Institutional Animal Care and Use Committee (protocol: 2002–04, 2025–521, 2408–04) reviewed and approved the protocol for all conducted experiments. Studies were performed in accordance with Canadian Council on Animal Care guidelines. For each study, three beagle dogs (age: 12–24 months, weight: 8.5–10 kg) were used (n = 3). They received food twice daily, while they were fasted for 2 to 3 h before application of patches or the BMT sc formulation and overnight before BMT capsule administration. For suction patch application, the dogs were anesthetized using 0.4 mg/kg torbugesic (Zoetis), 0.02 mg/kg acepromazine (Boehringer Ingelheim), 4 mg/kg propofol (Fresenius Kabi), and 0 or 0.01 mg/kg glycopyrrolate (Sandoz). The SMG- or BMT-containing patches (Section 2.18) were manually applied to the beagle dogs' buccal mucosa following mucosal wetting with DI water to counteract reduced salivation caused by anesthesia and were gently removed after 10 or 20 min. For oral delivery of capsules containing BMT, each dog received one capsule with 10 mL of tap water. The sc formulation of BMT was administered in the interscapular region as a single injection of 0.5 mL per dog (corresponding to a dose of 0.525 mg BMT) using a 1-mL syringe and 25G x 1 needle. Blood samples (4.5 mL) were taken into K_2EDTA tubes (BioIVT) at predefined time points. For SMG studies, samples were withdrawn at the following time points: 0, 15, 30, 60, 90, 150 (2.5 h), 240 (4 h), 360 (6 h), 1440 (24 h), and 4320 min (72 h) after application. For BMT capsules and patches, samples were taken at the following time points: 0, 15, 30, 60, 90, 150 (2.5 h), 240 (4 h), and 480 min (8 h), while for the BMT sc formulation, the time points were set at 0, 6, 15, 30, 60, 120 (2 h), 240 (4 h), and 480 min (8 h) post-dosing. After centrifuging blood aliquots at 1700 ×*g* for 10 min at 4 °C (Sorvall, ThermoFisher), plasma samples were stored at −80 °C until analysis (Platform of Biopharmacy, Faculty of Pharmacy, University of Montréal, Montréal, Québec, Canada). The Microsoft Excel Plugin PKSolver [59] was used for PK analysis. Additionally, photographs of the application sites were taken before, during, and after patch application.

2.20. Plasma concentration and residue analysis of SMG

SMG plasma concentrations were measured using strong ion exchange solid-phase extraction (SPE) and ultra-performance liquid chromatography (UPLC) coupled with quadrupole time-of-flight (QTOF) mass spectrometry (MS) in pseudo-multiple reaction monitoring (pseudo-MRM) mode. For sample extraction, 15 µL liraglutide (internal standard (IS), 8000 ng/mL in 1:1 (v/v) ACN/water solution) and 500 µL ACN/MeOH (1:1 v/v) were added to 250 µL of each dog plasma sample, followed by mixing. Samples were then centrifuged at 15′871 ×*g* (Eppendorf Microcentrifuge, Model 5424) for 5 min. From the resulting supernatant, 600 µL were diluted with 1.2 mL of 10% (v/v) NH_4OH aqueous solution in a 96-well plate. After conditioning SPE wells (Oasis MAX 96-well plate SPE plate 10 mg, 30 µm, Waters) with 500 µL of MeOH and 500 µL of 4% (v/v) NH_4OH aqueous solution, 1.8 mL of samples was loaded and aspirated through the SPE bed with low vacuum. Afterward, washes were performed with 500 µL of 4% (v/v) NH_4OH aqueous solution, 500 µL of ACN/water (20:80 v/v) containing 4% (v/v) NH_4OH, and lastly 200 µL of water supplemented with 2% FA. Finally, samples were eluted with 300 µL MeOH with 5% FA using low vacuum in a 96-well collection plate (QuanRecovery with MaxPeak, 700 µL, Waters) and diluted with 200 µL of water. For chromatographic analysis, 4–5 µL of each sample were injected into the UPLC system (Acquity UPLC I-Class, Waters) coupled to a high-resolution MS (Xevo G2-XS QTof, Waters) and ionized by electrospray ionization (ESI) in positive ion mode. A C18 column (Acquity UPLC BEH C18 130 Å, 50 mm × 2.1 mm, 1.7 µm, Waters) was used with two eluents; water with 0.1% (v/v) FA (mobile phase A) and ACN with 0.1% (v/v) FA (mobile phase B), while a flow rate of 0.4 mL/min and column temperature of 60 °C were applied. After initial equilibration at 20% (v/v) of mobile phase B, a gradient was used to reach 30% (v/v) B over 0.5 min, followed by 2.5 min of increasing B to 65% (v/v). After an increase to 98% (v/v) B in 0.2 min, a plateau at 98% (v/v) B was kept for 0.8 min, followed by a decrease to 20% (v/v) B over 0.1 min and equilibration for 1.2 min. The lower limit of quantification (LLOQ) was 2.4 ng/mL, as defined by the lowest calibrator within ± 20% of the nominal concentration. Values below LLOQ at $t = 0$ were set to 0 before further PK analysis. Calibration curves in a range of 2.4 to 400 ng/mL were plotted using the ratio of the analyte over IS peak area, with a quadratic regression with $1/x$ weighting factor.

Additionally, residues of SMG recovered after patch application were extracted by adding 4 mL of 20:80 (v/v) ACN/aqueous Tris buffer at pH 7.4 in a 5-mL Five-O™ tube (MTC Bio), followed by vortexing. After 5000-fold dilution in dog plasma, samples were injected into the UPLC system and analyzed as described for SMG plasma samples.

2.21. Plasma concentration and residue analysis of BMT

BMT plasma concentrations were analyzed using protein precipitation followed by UPLC/QTOF-MS in MRM mode. For sample extraction, 50 µL of each dog plasma sample were mixed with 100 µL of diltiazem (IS, 100 ng/mL) in ACN/MeOH (80:20 v/v) containing 0.1% FA. Then, the samples were centrifuged at 15′871 ×*g* (Eppendorf Microcentrifuge, Model 5424) for 4.5 min followed by diluting 75 µL of supernatant with 75 µL water containing 0.1% FA and transferring the extracts into a 96-well plate. For chromatographic analysis, 6–8 µL of each sample were injected into the UPLC-MS system and ionized by ESI in positive ion mode. A C8 column (Acquity UPLC BEH C8 130 Å, 50 mm × 2.1 mm, 1.7 µm, Waters) was used with a guard column (Acquity UPLC BEH C8 VanGuard Pre-Column, 130 Å, 5 mm × 2.1 mm, 1.7 µm, Waters) at 55 °C. The two eluents used were water with 0.1% (v/v) FA (mobile phase A) and ACN/2-propanol (80:20 v/v) with 0.1% (v/v) FA (mobile phase B). After isocratic equilibration at 15% (v/v) of mobile phase B for 1 min at 0.4 mL/min, an elution gradient was applied over 1.9 min at 0.4 mL/min to 48% (v/v) of B, followed by an increase to 99% (v/v) over 0.1 min with an increased flow rate of 0.5 mL/min. A plateau at 99% (v/v) B was held for 2.7 min at 0.5 mL/min before decreasing the flow rate back to 0.4 mL/min and eluent B to 15% (v/v) over 0.1 min and subsequent equilibration for 1.2 min. The LLOQ was 0.5–2 ng/mL, as determined by the lowest calibrator within ± 20% of the nominal concentration. Values below LLOQ at $t = 0$ were set to 0, while all other values below LLOQ were set to LLOQ/2 before further PK analysis. Calibration curves in a range of 0.5–2 to 400 ng/mL were plotted using the ratio of the analyte over IS peak area, with a quadratic regression with $1/x$ weighting factor.

The relative bioavailability (F_{rel}) (%) *vs.* the sc injection was calculated from the area under the concentration *vs.* time curve from 0 to 8 h ($AUC_{0\text{–}t}$) of the sc ($AUC_{0\text{–}t\ (sc)}$) and patch or capsule ($AUC_{0\text{–}t\ (patch/capsule)}$) formulations, as well as the doses for sc ($Dose_{(sc)}$) and patch/capsule ($Dose_{(patch/capsule)}$) formulations according to eq. (9).

$$F_{rel} = \frac{AUC_{0\text{–}t\ (patch/capsule)} \times Dose_{(sc)}}{AUC_{0\text{–}t\ (sc)} \times Dose_{(patch/capsule)}} \times 100 \quad (9)$$

Additionally, residues of BMT recovered after patch application were extracted by adding 4 mL of 20:80 (v/v) ACN/water supplemented with 0.1–2% FA and 0–0.1% OGP in a 5-mL Five-O™ tube (MTC Bio), followed by vortexing. After diluting 3000-fold in dog plasma, samples were injected into the UPLC system and analyzed as described for BMT plasma samples.

2.22. Statistical analysis

All data are presented as mean with standard deviation (SD) from at

least three independent replicates, as detailed in each figure description. GraphPad Prism (version 10, GraphPad Software) was used for statistical analysis. Statistical significance was calculated by one-way analysis of variance (ANOVA) with Tukey's multiple comparisons test, Welch's ANOVA with Dunnett's T3 multiple comparisons test in the case of unequal variance across groups, or by *t*-tests, as indicated in each figure description. Paired tests were used when comparing measurements taken from the same subjects under different conditions. A p-value < 0.05 was considered significant (visualized by $*p < 0.05$, $**p < 0.01$, $***p < 0.001$, $****p < 0.0001$).

3. Results

3.1. Characterization of poly(DLLA-co-CL) MA

We recently reported that the mechanical properties and degradation rates of DLP 3D-printed objects based on star-shaped/linear poly(DLLA-*co*-CL) MA mixtures could be modulated by adjusting the composition, ratios, and MW of the copolymers [51,52]. Inspired by these findings, we investigated whether such polymers, once thermally crosslinked, could match the mechanical properties of the previously reported non-degradable SCOD prototypes [48,49], and enable the production of an environmentally friendly alternative produced by a scalable molding process. Linear (P1) and star-shaped (P2) poly(DLLA-*co*-CL)s with a MW of 15 kDa were synthesized by $Sn(Oct)_2$-catalyzed ROP and functionalized with methacrylates (degree of methacrylation *ca.* 95%) (Figs. S1–4, Table S1). All polymers were amorphous, viscous liquids at RT (Fig. S11A and B).

Since branched polymers have more end groups available for crosslinking than linear polymers of the same MW, we created a crosslinking gradient by using resins with varying mass ratios of P1 (linear) to P2 (branched). The resins were prepared by mixing the polymers with the reactive diluent NVP (NVP:polymer 15:85 m/m) and a radical inhibitor, vitamin E (0.25 m%). At a temperature of 60 °C, all resins exhibited characteristics of viscous fluids, with viscosities ranging from *ca.* 56 Pa·s for resin of P1 alone down to *ca.* 32 Pa·s for the 60:40 P1:P2 mixture (Fig. 2A). Such viscosities are compatible with molding processes, as they allow both degassing and reshaping of the material. Thermal crosslinking in molds for dogbone-shaped test strips was then initiated by adding the radical initiator AIBN (0.5 m%), resulting in amorphous objects with T_gs of around −40 °C (Fig. S11C). The successful crosslinking of polymer end groups was confirmed by the absence of double bonds in molded objects compared to the original resin mixtures (Fig. S12).

The mechanical properties of crosslinked objects were evaluated by tensile testing of dogbone-shaped test strips (Fig. 2B–D). Objects composed of P1 alone displayed the highest elongation at break of 260%, while the incorporation of P2 at 40 m% significantly reduced this value to around 150% (Fig. 2C, p-value of 0.019). Concurrently, Young's modulus increased from 1.6 to 1.9 MPa when increasing the P2 content (Fig. 2D), attributed to its branched structure leading to higher crosslinking densities. These findings suggested a modest degree of tunability of mechanical properties within the tested material range. However, all obtained materials showed elasticity similar to the reference polymer

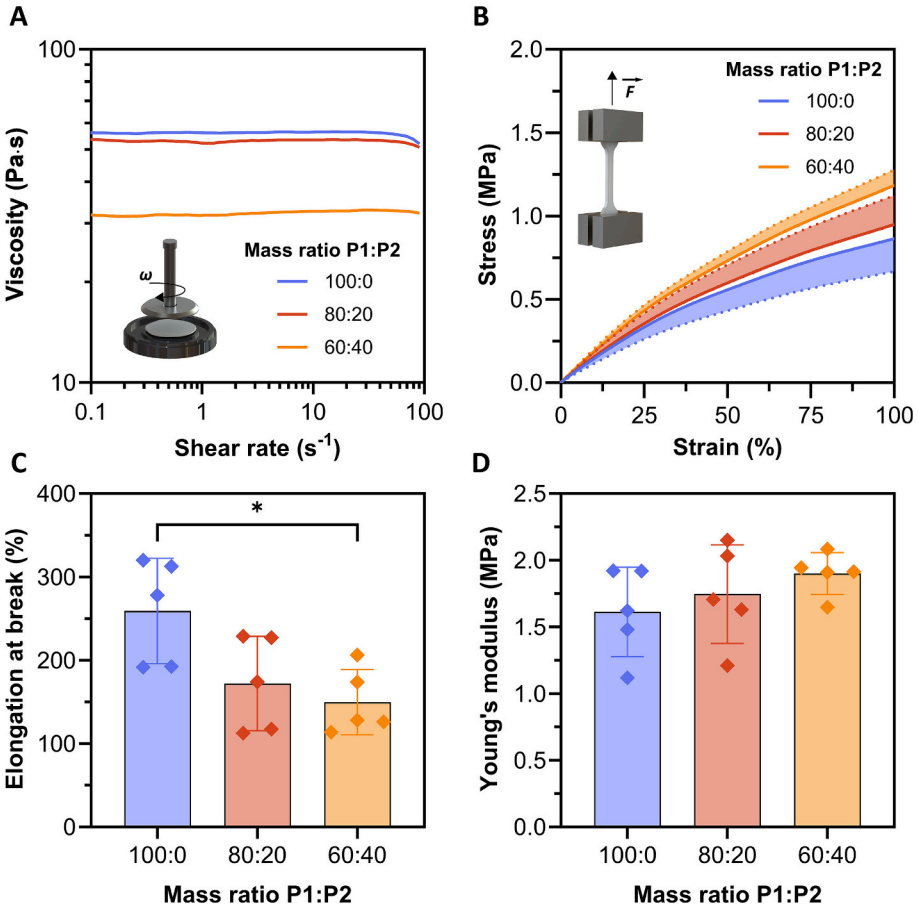

Fig. 2. Characterization of poly(DLLA-*co*-CL) MA. A) Representative viscosity measurements of resins with different mass ratios of linear (P1) to star-shaped (P2) polymer at 60 °C. B) Stress-strain curves up to 100% of strain, C) elongation at break, and D) Young's modulus of test strips produced from resins with different P1:P2 mass ratios. Data in B are presented as mean + standard deviation (SD) or mean - SD for clarity, and in C and D as mean ± SD (n = 5). Young's modulus in D was calculated from 0.325 to 0.925% strain. Data in C and D were analyzed using one-way analysis of variance (ANOVA) with Tukey's multiple comparisons test and statistically significant comparisons are indicated with $*p < 0.05$.

used for 3D printing of the initial SCOD prototype, which exhibited a Young's modulus of *ca.* 1.8 MPa and an elongation at break of 175% [48]. Therefore, all three materials would be suitable for SCOD fabrication.

3.2. Characterization of poly(DLLA-co-CL) MA patches

The next steps included the production and characterization of SCODs produced by molding of thermally crosslinked biodegradable copolymer resins (Fig. S5). First, to confirm the degradability of SCODs, the latter were incubated in PBS at 50 °C, and their mass and swelling were monitored over time (Fig. S13). In the first two weeks, no

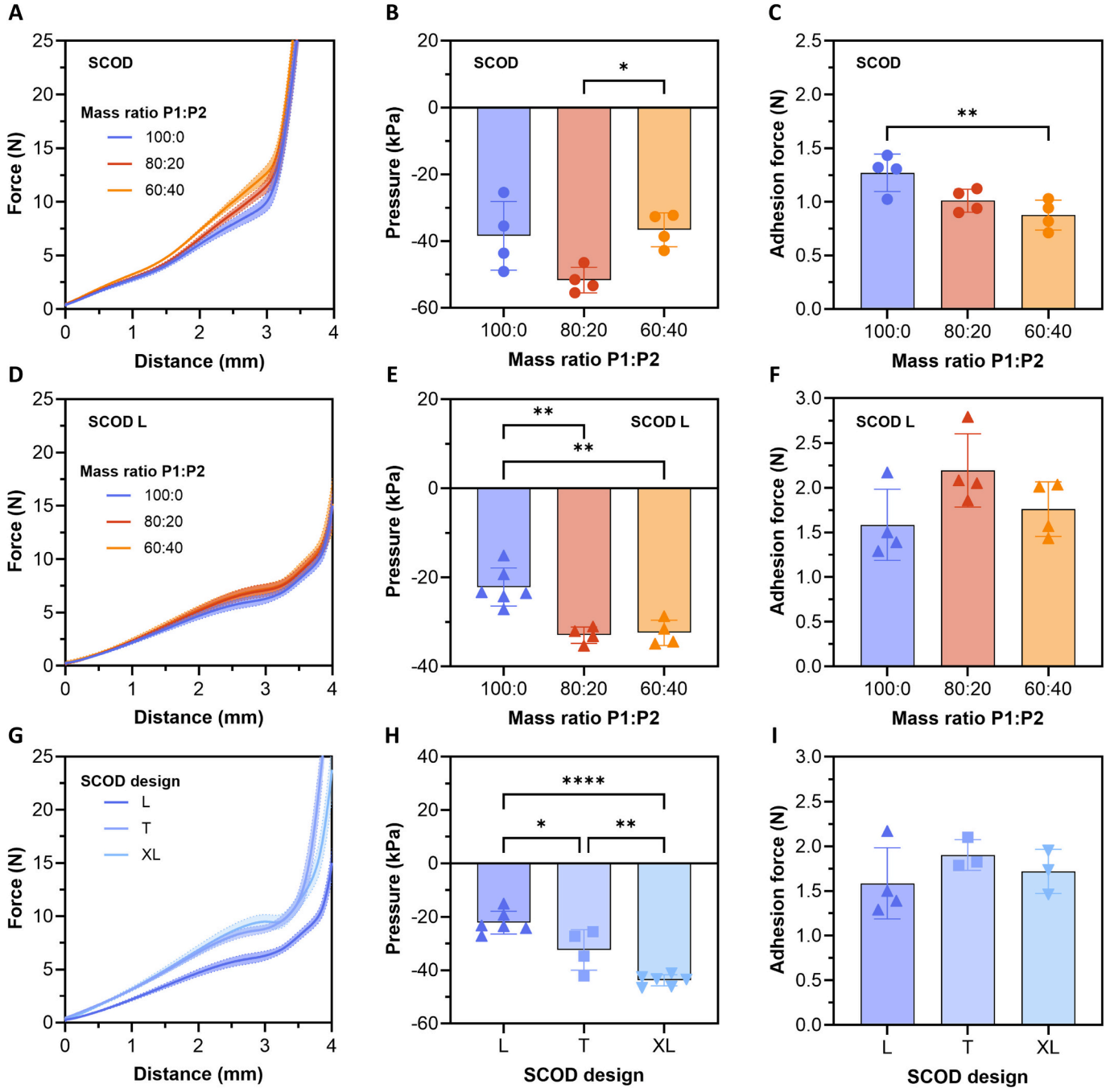

Fig. 3. Mechanical performance of poly(DLLA-*co*-CL) MA SCODs of different material/design combinations. A) Compression force-displacement curves (n = 5 for P1:P2 100:0 and n = 4 for P1:P2 80:20 and 60:40 m/m), B) average negative pressure over 10 min (n = 4), and C) adhesion force on Shore A (ShA) 00 silicone at 0° (n = 4 with three measurements per patch) of SCOD patches made of resins with different P1:P2 mass ratios. D) Compression force-displacement curves (n = 6 for P1:P2 100:0, n = 4 for P1:P2 80:20 and 60:40 m/m), E) average negative pressure over 10 min (n = 4–6), and F) adhesion force on ShA 00 silicone at 0° (n = 4 with three measurements per patch) of SCOD L patches made of resins with different P1:P2 mass ratios. G) Compression force-displacement curves (n = 6 for SCOD L and SCOD XL, n = 4 for SCOD T), H) average negative pressure over 10 min (n = 4–6), and I) adhesion force on ShA 00 silicone at 0° (n = 3–4 with three measurements per patch) of different SCOD designs made of P1. All data are expressed as mean ± SD. Note that the data in G to I for SCOD L are the same as for P1:P2 100:0 in D to F. Data in B, C, E, F, H, and I were analyzed using one-way ANOVA with Tukey's multiple comparisons test and statistically significant comparisons are indicated with $*p < 0.05$, $**p < 0.01$, $****p < 0.0001$.

differences were observed among the tested materials. However, after four weeks, three SCODs of P1 collapsed, while the only P1-SCOD retrievable from the buffer demonstrated a mass loss of 25%. During the same time, devices made of P1:P2 80:20 lost 30% of their mass on average. In contrast, the ones made from P1:P2 60:40 remained at only 13% loss (Fig. S13A). The SCODs based on P1 only and the P1:P2 80:20 mixture also exhibited higher water uptake and faster acidification of the degradation medium than those with higher P2 content (Fig. S13B and C). Photographs confirmed that devices with higher P2 content maintained their structural integrity for up to five weeks, whereas SCODs made of P1 only and P1:P2 80:20 started to collapse after three and four weeks, respectively (Fig. S13D). Therefore, the degradability of thermally crosslinked objects was confirmed.

To identify the best-performing device, both the SCOD and the larger SCOD L design [49] were produced with different resins and characterized across a range of mechanical tests. In uniaxial compression tests performed on a 3D-printed platform (Fig. S6), P1 devices had the lowest compression resistance at given distances (Fig. 3A and D), especially for SCOD (Fig. 3A), which aligned with the highest elasticity observed in tensile tests. The lower overall compression resistance of the SCOD L can be attributed to its larger inner compartment volume, making the differences caused by the material composition less pronounced (Fig. 3D). Then, the negative pressure induced by the device application was assessed (Fig. 3B and E, Fig. S7). While for the SCOD, the P1:P2 80:20 devices displayed the lowest negative pressure of *ca.* −52 kPa, followed by P1 (−38 kPa) and then P1:P2 60:40 (−37 kPa), both mixtures with P2 performed better than P1 alone for SCOD L (*ca.* −32 kPa for 80:20 and 60:40 P1:P2 *vs.* −22 kPa for P1-only). This coincides with our previous observations that stiffer elastic materials are preferred for the manufacturing of the SCOD L device [49]. Further, adhesion tests were carried out on a soft silicone surface to evaluate the maximum adhesion strength of patches (Fig. 3C and F, Fig. S8). In the SCOD case, P1 alone outperformed P1:P2 mixtures with a vertical adhesion force up to *ca.* 1.3 N, which closely resembles the results obtained with the original 3D-printed prototype (1.2–1.4 N), as well as optimized PDMS-based SCODs (1.5 N for the best-performing PDMS with ShA 30) [48,49]. In the case of SCOD L, the P1:P2 80:20 patch was the best-performing one, achieving values as high as 2.2 N, matching the best-performing PDMS-based device (2.2 N) and even surpassing the 3D-printed SCOD L (1.7 N) [49]. The improved adhesion of SCOD L devices can be explained by their larger surface contact area. Interestingly, in angled adhesion experiments at 45° (Fig. S8B), differences between SCOD patches of different materials were insignificant (Fig. S14A), while for SCOD L, the P1:P2 80:20 mixture showed significantly (*p*-values of 0.006–0.008) lower adhesion than P1:P2 60:40 and P1 alone (*ca.* 1.3 *vs.* 1.6 N) (Fig. S14B).

Since all biodegradable devices exhibited mechanical properties generally comparable to the initial SCOD prototype, with only minor variations due to resin composition, no single material clearly emerged as the best performer. However, devices containing P2 broke after only a few compressions, while the devices made from P1 alone were more resistant. This was particularly evident in SCOD L, where thinner walls at the orifice increased the device's susceptibility to failure with less elastic materials. Therefore, we sought to adapt the SCOD L – the prototype associated with the highest bioavailabilities to date [49] – to the P1 polymer by slightly increasing the wall thickness to enhance the resistance to compressive forces. To this end, two new designs were generated: the SCOD T with thicker walls (1.55 instead of 1.4 mm) at constant height (6.5 mm) and the SCOD XL with thicker walls (1.55 mm) at increased height (6.65 mm). Uniaxial compression tests confirmed the increase in material resistance, while near-complete compression of novel designs was still achieved at forces comparable to those required for complete compression of SCOD L (Fig. 3G). The negative pressure generated with new designs was also improved, with SCOD T reaching −32 kPa and SCOD XL nearly doubling the negative pressure of SCOD L, at −44 kPa (Fig. 3H). However, both vertical (Fig. 3I) and angled adhesion tests (Fig. S14C) revealed insignificant improvements in adhesion over SCOD L. Based on these findings, we prioritized the larger designs SCOD L, T, and XL and selected P1-only-based material to be further evaluated for biodegradable patch production.

3.3. Disintegration in environmental conditions

As our ultimate goal was to create a compostable, low-waste version of the patch, we proceeded with testing the disintegration of selected P1-polymer-based material under simulated compost conditions. We incubated thermally crosslinked sheets made entirely of P1 (25 × 25 × 1 mm, *ca.* 600 mg) in synthetic waste at 58 °C, following the procedure outlined in ISO 20200:2015. Within a few days, the sheets began absorbing moisture and became sticky, making it difficult to separate them from the compost without damage (Fig. 4, Fig. S15). From 30 days onwards, according to ISO 20200:2015, no more water had to be added to the mixtures, as the total mass was constantly above 80% of the original mass. This led to the samples drying out completely. After 60 days, the residual pieces distinguishable from the compost were collected and cleaned, and their final weight was determined. With a drop in average absolute weight to *ca.* 320 mg (Fig. S16A), an average disintegration degree of 48% after only 60 days was achieved, indicating moderate disintegration over time in simulated waste (Fig. S16B).

3.4. Ex vivo performance on porcine buccal mucosa

In the next testing phase, SCOD L, SCOD T, and SCOD XL patches made of P1 were applied to freshly excised porcine buccal mucosa to determine whether their application would induce tissue deformation and enhance the permeability of Cy5, a poorly permeable fluorescent dye. Mold-cast PDMS ShA 50 SCOD L patches, both with and without NaTaC (+PE and -PE), were included as control formulations [48]. After 30-min patch application at 37 °C, the SCOD L PDMS -PE control produced no visible permeation of Cy5 (red) into the tissue (Fig. 5A) [48]. The positive control of SCOD L PDMS +PE, as well as all three P1-based SCODs, showed Cy5 fluorescent signal within the region of deformation, confirming our previous observation that mechanical stretching alone does not substantially enhance permeation, whereas the combination with PEs (*i.e.*, NaTaC, 3 mg) significantly improves diffusion [48,49]. Cy5 fluorescence intensity profiles in Fig. 5A were quantified as a function of distance from the tissue outline (Fig. S9, Fig. S17A–E) as described in Section 2.16 and used to determine the maximum d_p, a parameter indicative of overall permeation enhancement (Fig. 5C). While the control PDMS device without PE (SCOD L PDMS -PE) exhibited a d_p of only 700 μm, adding PE increased the d_p to nearly 2100 μm (SCOD L PDMS +PE). The biodegradable devices reached d_p values ranging from 1480 to 1600 μm, with SCOD XL +PE showing a significant improvement over SCOD L PDMS -PE (*p*-value of 0.03). Considering the buccal epithelial thickness (500–800 μm [32,48]), d_p-values beyond this threshold are interpreted as indicative of sufficient permeation, demonstrating the suitability of PE-containing devices over the negative control.

This trend could also be observed when comparing the cumulative AUC (*cAUC*) of different segments *vs.* $cAUC_{0–3000}$ of the fluorescence intensity profiles (Fig. S17F, Table S3). The *cAUC* of the first segment from 0 to 500 μm was the largest for the PDMS control without PE (71% of $cAUC_{0–3000}$), indicating that Cy5 was mostly found at the surface of the tissue. The addition of NaTaC to the formulation led to increased percentages for all segments after 500 μm, while the value of the first segment was reduced to around 65%, irrespective of the patch used. Therefore, the cumulative Cy5 signal in deeper tissue was consistently higher for patches with PE compared to the control patch without PE (Fig. S17F).

This *ex vivo* setting was also used to assess tissue deformation upon patch application. Histochemical staining of F-actin (green) and the nuclei (blue) was performed to enhance the visibility of the outline of deformation (Fig. 5B). All samples showed adequate suction of the tissue

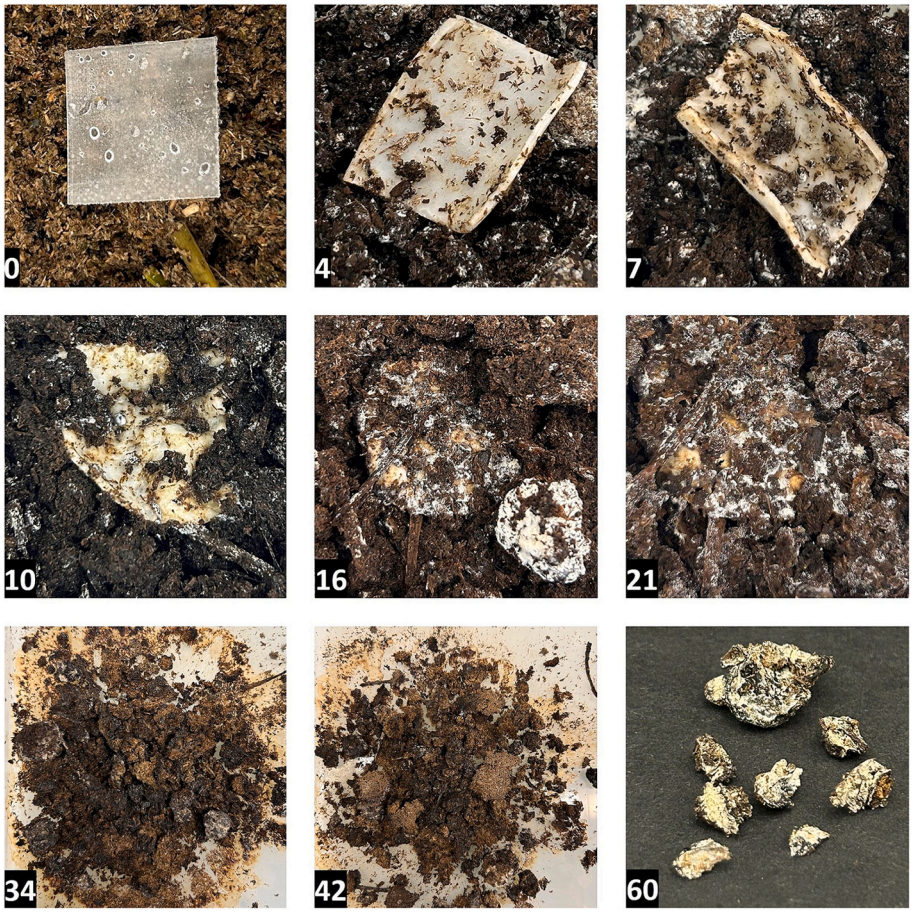

Fig. 4. Disintegration in synthetic waste. Visual progression of the degradation process of a representative sheet made of thermally crosslinked P1 at different time points during incubation in synthetic waste at 58 °C (number of days indicated at the bottom left of each picture). The full panel with all six samples can be found in the Supporting Information (Fig. S15).

into the devices. As shown in Fig. 5D, the calculated *SE* (Section 2.17) ranged between 58 and 72%, with no significant differences among the various devices produced with either PDMS or P1. This shows that the stretching achieved by biodegradable devices was comparable to that of PDMS devices upon application to porcine tissue. Collectively, these results indicate that, *ex vivo,* the biodegradable prototypes made of P1 are comparable to non-degradable PDMS devices in both permeation enhancement and *SE*.

3.5. *In vivo performance in beagle dogs*

Finally, the *in vivo* performance of the biodegradable SCOD was assessed in beagle dogs with the P1-based SCOD XL prototype, as it was associated with the highest negative pressure (Fig. 3H), suitable adhesion force (Fig. 3I and Fig. S14) and resistance to uniaxial compression (Fig. 3G), as well as *ex vivo* functionality (Fig. 5) (Table S4). Before the *in vivo* testing, we evaluated the stability of patches stored under ambient conditions (RT) or vacuum. While the resistance to uniaxial compression was preserved over three months under vacuum (Fig. S18A), a gradual decrease in resistance with time was observed under ambient conditions, indicating softening of the patches (Fig. S18B). Consequently, patches selected for *in vivo* studies were freshly prepared and used immediately after manufacturing or stored under vacuum before use.

First, the biodegradable SCOD XL was loaded with 2 mg SMG, 0.4 mg PVA as matrix polymer, and 3 mg NaTaC as the PE. The resulting PK profile was compared to that of a control PDMS SCOD L loaded with the same formulation (Fig. 6A). The latter was selected due to its previously demonstrated ability to achieve the highest SMG absorption [49]. The patches were applied to the dog's cheek mucosa for only 10 min. Both devices performed similarly with maximum observed plasma concentrations (C_{max}) of 175 and 151 ng/mL for the PDMS SCOD L and P1-SCOD XL, respectively (Table S5). Concurrently, the dose-adjusted total area under the concentration *vs.* time curve ($AUC_{0-\infty}$) was 5429 and 4076 ng*h/mL/mg for PDMS SCOD L and biodegradable SCOD XL, respectively (Fig. 6B). In relation to our previously published data, only a slight decrease in dose-adjusted $AUC_{0-\infty}$ of SMG delivered *via* SCOD L PDMS was observed when reducing the application time from 30 to 10 min [49]. However, compared to the Rybelsus® tablet, a 7 to 9-fold increase in dose-adjusted $AUC_{0-\infty}$ was achieved for the biodegradable SCOD XL and PDMS SCOD L, respectively [49]. The tolerability of the P1-SCOD XL applied with SMG and NaTaC for 10 min was visually confirmed by photographs taken at the application site (Fig. S19). While slight redness could be seen immediately after removing the patches, the tissue completely recovered 24 h after the application, without any signs of persisting irritation.

Finally, we used the biodegradable patch to deliver another peptide, the melanocortin receptor agonist BMT (1.03 kDa, $t_{1/2}$ = 2–4 h), which is currently only available as an injectable for sc administration (Fig. 6C). SCOD XLs were loaded with 2 mg of BMT (with or without mannitol) and 3 mg C10 as PE (Fig. 6D). C10, which also promotes transbuccal absorption *ex vivo* when loaded in SCODs [48], was used as the PE in this case, as precipitation was observed when combining NaTaC with BMT. The BMT PK profile was first obtained after the application of BMT (containing mannitol)-loaded P1-SCOD XL for 10 min and compared to PK profiles generated after sc injection of the solution (Fig. 6C) and oral administration of enteric capsules (Fig. 6E). The

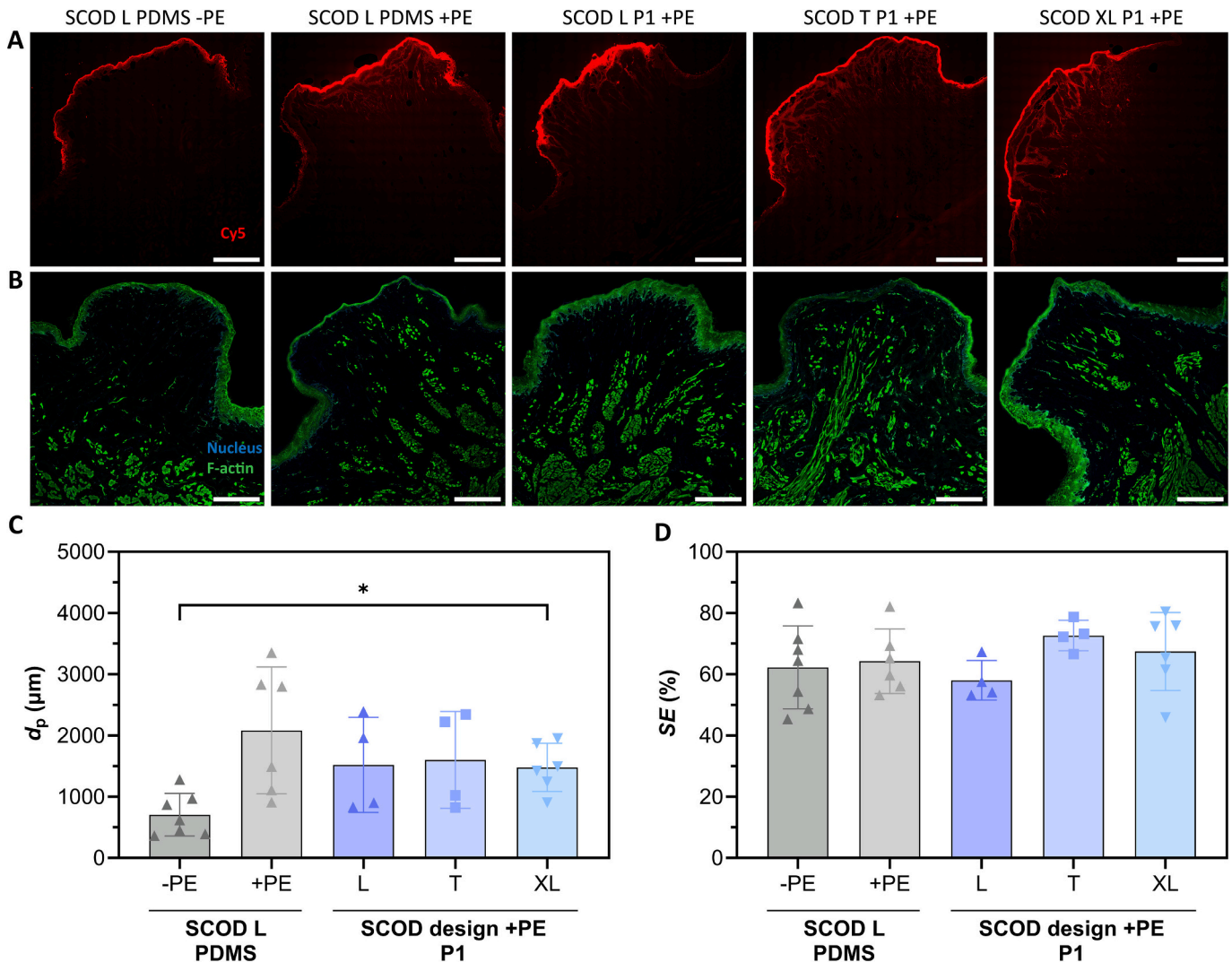

Fig. 5. *Ex vivo* characterization of SCODs of various designs after application on porcine buccal mucosa. A) Representative fluorescent microscopy images of cryosectioned porcine buccal tissue after application of cyanine 5 (Cy5)-loaded patches (Scale bar: 2 mm). B) Representative microscopy images of deformed tissue caused by patch application, as visualized by histochemical staining with Hoechst for cell nuclei (blue) and phalloidin-iFluor 488 reagent for F-actin (green) (Scale bar: 2 mm). C) Maximum penetration depth (d_p) quantified based on microscopy images as shown in A using Python to obtain fluorescence intensity profiles. A threshold of 0.025 was set on normalized fluorescence intensity profiles (Fig. S17) to obtain d_p values. D) The stretching efficiency (*SE*) as a ratio between the final (SA_{final}) and maximal surface area (SA_{max}) was obtained from histochemically stained microscopy images as shown in B using ImageJ and SolidWorks (Fig. S10). Biodegradable SCOD L, SCOD T, and SCOD XL patches made of P1 were loaded with 0.4 mg poly(vinyl alcohol) (PVA), 54 µg Cy5, and 3 mg sodium taurocholate (NaTaC) per patch, while SCOD L poly(dimethylsiloxane) (PDMS) patches were applied both with 3 mg and without NaTaC as controls. All patches were applied for 30 min at 37 °C on freshly excised porcine buccal mucosa. Note that the images in A and B were cropped for demonstration, and brightness/contrast settings for A were adjusted equally, while in B, brightness/contrast were adjusted on a per-image basis for visualization purposes. Original microscopy images can be found in the raw data. Data in C and D are expressed as mean ± SD (n = 4–7) and were analyzed using Welch's ANOVA with Dunnett's T3 multiple comparisons test (C) or one-way ANOVA with Tukey's multiple comparisons test (D), and statistically significant comparisons are indicated with $*p < 0.05$. (For interpretation of the references to colour in this figure legend, the reader is referred to the web version of this article.)

capsules were administered with 2 mg of BMT (containing mannitol) and either no PE or 250 mg C10, an amount of PE comparable to that used in peptidic oral formulations [60]. The application of P1-SCOD XL for 10 min increased the AUC_{0-t} 15-fold and 1.7-fold compared to capsules without and with PE, respectively. The F_{rel} *vs.* the sc formulation was 9.4, 0.6, and 5.4% for the SCOD XL (10 min) and capsules without or with C10, respectively (Fig. 6F and Table S6).

However, while the formulations were shown to be well tolerated, with swelling and redness disappearing within 24 to 72 h post-removal (Fig. S20A), the images indicated incomplete dissolution of the loaded formulation. Given the limited saliva volume available at the mucosal surface (50 µm thick saliva film providing *ca.* 2.5 µL [61]), the presence of high amounts of mannitol (*i.e.*, 8 mg at a dose of 2 mg BMT) in the purchased BMT (UK Peptides) may have hindered complete drug dissolution. To further boost BMT transbuccal absorption, it was decided to prolong the application time and change the source of BMT to a different supplier (Toronto Chemicals), affording the BMT without any mannitol. As shown in Fig. 6D and F and Table S6, applying the mannitol-free formulation for 20 min resulted in a F_{rel} of 26% compared to the sc solution, clearly demonstrating the good transbuccal absorption of BMT with the biodegradable SCOD. Images taken during and after the cup application showed improved dissolution as compared to the 10-min application (Fig. S20B), while the recovered BMT in the cup was reduced from 1.37 mg for the 10-min to 0.88 mg for the 20-min application (Table S6). After a maximum of six days post-removal, there was no visible sign of irritation in any of the dogs, confirming

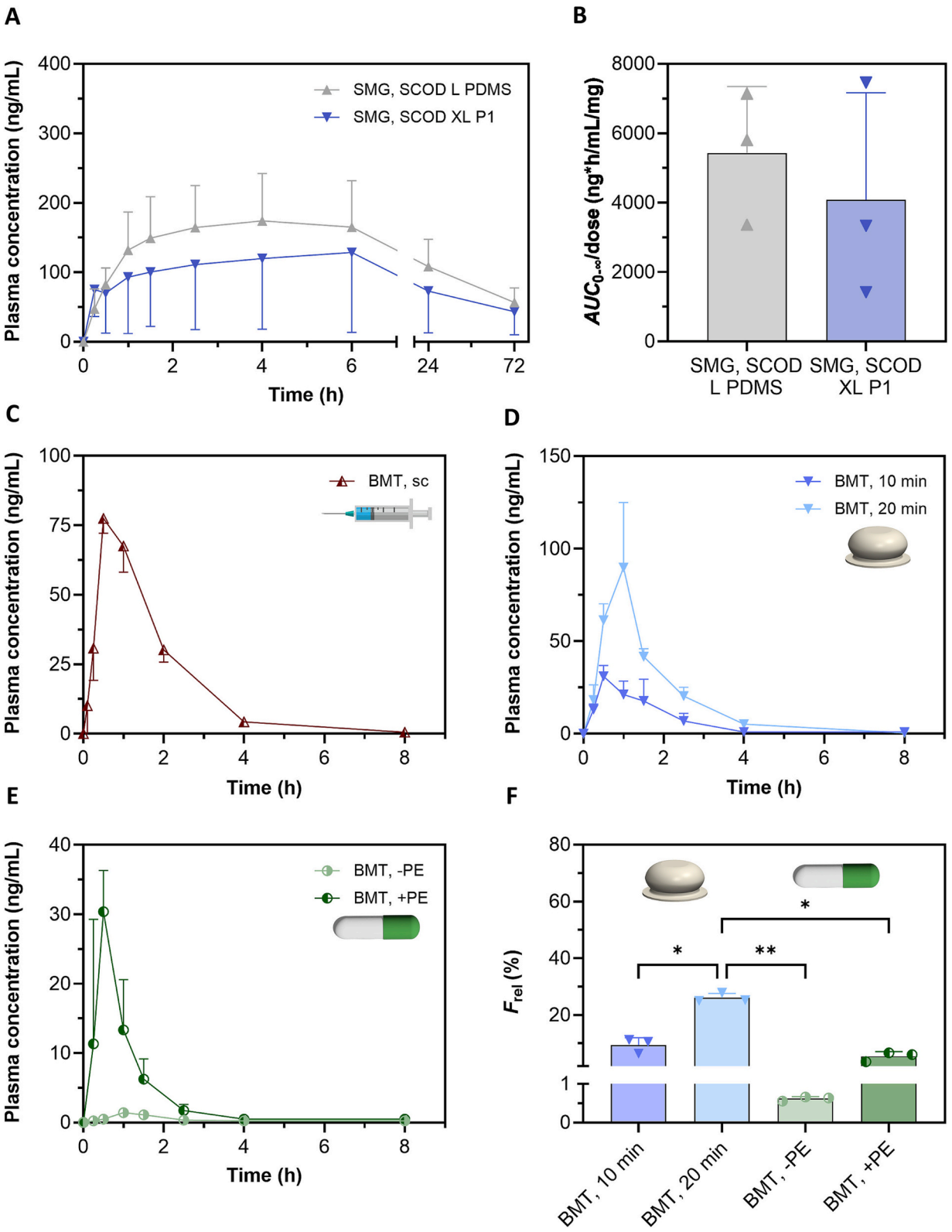

Fig. 6. Pharmacokinetic (PK) studies of peptides in beagle dogs. A) Plasma concentration of semaglutide (SMG) after 10-min applications of SCOD L made of PDMS and SCOD XL made of P1, both containing 2 mg SMG, 0.4 mg PVA, and 3 mg NaTaC. B) Dose-adjusted total area under the concentration *vs.* time curve ($AUC_{0-\infty}$) derived from PK profiles shown in A. C) Plasma concentration of bremelanotide (BMT) after subcutaneous (sc) administration (0.525 mg). D) Plasma concentrations of BMT after application of SCOD XL made of P1, containing 2 mg BMT and 3 mg sodium decanoate (C10), and applied for 10 min (with mannitol) or 20 min (without mannitol). E) Plasma concentration of BMT after oral administration in capsules containing no permeation enhancer (PE) or 250 mg C10. F) Relative bioavailability (F_{rel}) (0–8 h) of BMT formulations in D and E relative to the sc formulation shown in C. All data are expressed as mean + SD or mean - SD for clarity (n = 3). Data in B were analyzed using a paired *t*-test, while data in F were analyzed using repeated measures one-way ANOVA with Tukey's multiple comparisons test, and statistically significant comparisons are indicated with $*p < 0.05$, $**p < 0.01$.

the tolerability of the formulation. Overall, these findings validate our hypothesis that biodegradable SCOD devices made of poly(DLLA-*co*-CL) MA can serve as interchangeable alternatives to PDMS devices for the systemic delivery of peptide drugs.

4. Discussion and conclusions

In this work, we present a sustainable alternative to the recently reported SCOD for transbuccal peptide delivery [48,49]. Poly(DLLA-*co*-CL) MA was selected as the starting material owing to its previously reported suitability for preparing 3D-printed biodegradable elastic objects with good mechanical resistance, especially when combining polymers of branched and linear structure [51,52]. In this case, the SCODs were not 3D printed but produced by mold casting followed by thermal crosslinking. The impact of P2 content on the mechanical properties was found to be moderate, with all tested materials closely matching previously 3D-printed prototypes in terms of elongation at break (175%) and Young's modulus (1.8 MPa) [48].

Mold-cast SCOD and SCOD L were nearly fully compressible at *ca.* 15–25 N, falling in the range of the force estimated to be created by a human finger compression (23 N) [62]. The generated negative pressure and adhesion force upon application onto soft silicone were also close to those of the original non-degradable prototypes [48,49]. However, P2-containing devices were prone to break at the orifice, whereas P1-only devices were found to resemble softer PDMS in compressive tests [49]. For SCOD L, it was reported that tougher materials were the best-performing ones [49], therefore, we optimized the SCOD L design by slightly increasing the wall thickness and base diameter and successfully increased the compressive resistance (Fig. 3G) and negative pressure of P1-based devices (Fig. 3H).

The degradation of the poly(DLLA-*co*-CL) MA SCOD was confirmed in PBS and simulated waste under stressed conditions. The P1-objects exhibited *ca.* 50% disintegration after only 60 days at 58 °C in simulated waste (Fig. 4). However, while the observed disintegration of the materials indicates the potential for environmental degradability, further testing is needed to align with established standards. For example, ASTM D6400–23 defines a material as compostable if, among other criteria, it disintegrates in a controlled simulated waste environment with no more than 10% of its original dry weight remaining after twelve weeks. In addition, the material must demonstrate adequate biodegradation, typically measured by the percentage of conversion to carbon dioxide (*e.g.*, according to ISO 14855–1 or ISO 14855–2), and must exhibit no ecotoxic effects. Therefore, future assessments should focus on specific biodegradation testing and fine-tuning of the SCOD composition to fully meet the compostability requirements outlined in ASTM D6400–23.

Ex vivo, the biodegradable SCOD enhanced the diffusion of the poorly membrane-permeable dye Cy5 across the porcine buccal mucosa, similar to the PDMS control. The efficiency of the device was then confirmed in dogs, first using SMG as a model peptide, given our former experience with this drug. However, compared to our recent study [49], we shortened the application time from 30 min to only 10 min in order to improve future patient acceptance. Both the PDMS and biodegradable devices performed similarly after buccal application, although the variability of the biodegradable device seemed to be higher. Importantly, more than 24 h post-application, no local irritation was observed with the biodegradable device in any of the dogs (Fig. S19), in line with our previous findings [49]. Compared to previously reported data of the PDMS patch with a 30-min application time, the reduction in dose-adjusted $AUC_{0-\infty}$ was approximately 9% for the PDMS patch and 32% for the biodegradable patch [49]. Interestingly, SMG dose-adjusted *AUC*s exceeded those of the Rybelsus® tablet by 7- to 9-fold (Fig. 6B) [49], indicating an advantage of the buccal patch over the commercial tablet formulation.

Additionally, we tested the biodegradable patch for the delivery of BMT, a newly marketed peptide that is approved for hypoactive sexual desire disorder in premenopausal women [63]. Notably, to make the device even more sustainable, we omitted the water-soluble matrix polymer PVA from the formulation, which was found to degrade very slowly and only in the presence of microorganisms [64]. After an application time of 20 min, the F_{rel} reached 26% (Fig. 6F, Table S6). This was nearly five times higher than the oral control capsule with C10, which contained over 80 times more PE. Further, the coefficient of variation (CV) was reduced by nearly 2-fold (43% for capsule *vs.* 25% for the 20-min patch). Compared to other previously published data dealing with the intranasal administration of BMT, indicating a bioavailability of *ca.* 7% in dogs [65], our findings suggest a substantial increase in F_{rel} when BMT was applied buccally with our patch. Additionally, no signs of irritation were observed in any of the dogs within six days following patch removal, further underlining the tolerability of the formulation (Fig. S20).

Beyond functional performance, environmental aspects of the formulation and its components should also be considered. Poly(DLLA-*co*-CL) MA was used as a proof-of-concept material for molding the devices, and while conventional synthesis of its monomers can involve environmentally taxing processes, efforts are ongoing to make their production more ecological [66,67]. The synthetic initiators that were used for copolymerization could be replaced with natural alternatives like glycerol, which was used in the preparation of similar polymer systems [68]. The catalyst used in the polymer synthesis, namely Sn $(Oct)_2$, is widely employed in ROP of DLLA, CL, and similar monomers due to its high reactivity, with regulatory acceptance within certain limits [69]. However, it is moderately toxic and not environmentally friendly, and could be replaced with more sustainable alternatives such as zinc- or iron-based catalysts [70,71]. The polymer synthesis itself is a solvent-free process, however, the functionalization to make the polymers crosslinkable involves the use of DCM, which should be replaced with greener solutions to increase the ecological benefit [72]. For example, supercritical carbon dioxide might be an alternative, due to its inertness and environmental benefit over conventional organic solvents [73,74]. To further improve the sustainability of the patch, other biodegradable polymer systems, such as poly(glycerol sebacate), could be integrated into the device design. This polyester is produced *via* high-temperature polycondensation, without solvents or catalysts, and enables crosslinking without additional initiators [75].

Collectively, we show that using biodegradable polymers can be a promising sustainable alternative to PDMS patches and other non-invasive buccal delivery systems, such as the MucoJet system, which comprises non-degradable plastic elements [46]. Similarly, other oral drug delivery devices under development, such as the self-orienting millimeter-scale applicator [21] or the luminal unfolding microneedle injector [25], while capable of delivering larger macromolecules, contain non-degradable components, such as metallic parts, rendering their conversion into environmentally friendly systems more complicated. It is worth noting that several other buccal or GI-based systems comprising degradable components are under development. For example, a microneedle-based peristalsis-actuated robot for GI-delivery incorporates biocompatible and degradable materials, like swellable carboxymethyl cellulose [24]. Targeting the buccal mucosa, dissolvable microneedle systems have also emerged as zero-waste approaches [44].

In conclusion, the data provided support the further development of biodegradable polymers for scalable and sustainable SCOD production. This study showed that the SCOD design can be finely tuned to compensate for any weaknesses in the material's physical properties, providing devices with proper elasticity, robustness, and mucoadhesion. Finally, the platform nature of the SCOD technology was further illustrated here. To the list of previously investigated peptides with non-degradable prototypes, *i.e.*, desmopressin, SMG, and teriparatide [48,49], we have now added BMT, demonstrating the biodegradable device's suitability for transbuccal delivery with an application time of less than 30 min. However, for successful clinical translation, further improvement of scalability will have to be addressed, either by enabling

faster crosslinking of the proposed polymers or by replacing them with injection-moldable materials to streamline production. Additionally, future studies should investigate the safety and tolerability of repeated patch administration. Overall, this work introduces a biodegradable SCOD, offering a non-invasive but also environmentally friendly approach for the systemic delivery of peptides and other macromolecules.

Declaration of AI and AI-assisted technologies in the writing process

During the preparation of this work, the authors used ChatGPT in order to support the writing and coding process. After using this tool/service, the authors reviewed and edited the content as needed and take full responsibility for the content of the publication.

CRediT authorship contribution statement

Hanna Krupke: Writing – original draft, Visualization, Methodology, Investigation, Formal analysis, Data curation, Conceptualization. **Nicole Zoratto:** Writing – review & editing, Validation, Methodology, Investigation. **Lucie Rabut:** Writing – review & editing, Investigation, Data curation. **Daniel Gao:** Writing – review & editing, Validation, Software. **Nevena Paunović:** Writing – review & editing, Supervision, Methodology, Funding acquisition, Conceptualization. **David Klein Cerrejon:** Writing – review & editing, Methodology, Funding acquisition, Conceptualization. **Benoit Dehapiot:** Writing – review & editing, Software, Data curation. **Jean-Christophe Leroux:** Writing – review & editing, Supervision, Resources, Project administration, Funding acquisition, Conceptualization.

Declaration of Competing Interest

JCL and DKC are co-inventors on patent applications related to the suction patch technology. JCL, DKC, and NP are shareholders in OBaris AG, a company developing the suction patch technology. The other authors declare no competing interests.

Acknowledgements

This research was supported by a grant from Innosuisse (106.899 IP-LS). NP acknowledges funding from the Gebert Rüf Foundation – Inno-Booster, and DKC from Swiss National Fonds Bridge – Proof of Concept Grant (222418). The authors thank Karen Dubé, Laurence Vivier (INRS), and Martin Jutras (University of Montréal) for their help in performing and analyzing *in vivo* experiments. Ronny Gunzenhauser, David Stapfer, Joel Friedli, and Denis Haxholli (Mechanical Workshop, ETH Zurich) are acknowledged for their support with mold manufacturing. The authors thank Wacker Chemie AG for providing medical-grade silicone. The authors further thank Hwangseok Kim and Eunsong Jung of Prof. Dr. Tae-Lim Choi's laboratory (ETH Zurich) for their help with SEC experiments, and Dr. Padryk Merkl and Méline Zhao for insightful exchange regarding the imaging data analysis. Schlachtbetrieb Zürich AG is acknowledged for supplying porcine buccal tissue.

Appendix A. Supplementary data

Supplementary data to this article can be found online at https://doi.org/10.1016/j.jconrel.2025.113947.

Data availability

The data that support the findings of this study are available in the ETH Research Collection.

References

[1] D.J. Brayden, T.A. Hill, D.P. Fairlie, S. Maher, R.J. Mrsny, Systemic delivery of peptides by the oral route: formulation and medicinal chemistry approaches, Adv. Drug Deliv. Rev. 157 (2020) 2–36.
[2] A.A. Kaspar, J.M. Reichert, Future directions for peptide therapeutics development, Drug Discov. Today 18 (2013) 807–817.
[3] M. Muttenthaler, G.F. King, D.J. Adams, P.F. Alewood, Trends in peptide drug discovery, Nat. Rev. Drug Discov. 20 (2021) 309–325.
[4] K.D. Stewart, J.A. Johnston, L.S. Matza, S.E. Curtis, H.A. Havel, S.A. Sweetana, H. L. Gelhorn, Preference for pharmaceutical formulation and treatment process attributes, Patient Prefer. Adherence 10 (2016) 1385–1399.
[5] C.V. Spain, J.J. Wright, R.M. Hahn, A. Wivel, A.A. Martin, Self-reported barriers to adherence and persistence to treatment with injectable medications for type 2 diabetes, Clin. Ther. 38 (2016) 1653–1664.e1.
[6] Overview of technologies for the treatment of infectious and sharp waste from health care facilities, World Health Organization, Geneva, 2019 (Licence: CC BY-NC-SA 3.0 IGO).
[7] D.J. Drucker, Advances in oral peptide therapeutics, Nat. Rev. Drug Discov. 19 (2020) 277–289.
[8] M. Goldberg, I. Gomez-Orellana, Challenges for the oral delivery of macromolecules, Nat. Rev. Drug Discov. 2 (2003) 289–295.
[9] C.K. Wang, J.E. Swedberg, P.J. Harvey, Q. Kaas, D.J. Craik, Conformational flexibility is a determinant of permeability for cyclosporin, J. Phys. Chem. B 122 (2018) 2261–2276.
[10] S. Maher, D.J. Brayden, L. Casettari, L. Illum, Application of permeation enhancers in oral delivery of macromolecules: an update, Pharmaceutics 11 (2019) 41.
[11] C. Granhall, M. Donsmark, T.M. Blicher, G. Golor, F.L. Søndergaard, M. Thomsen, T.A. Bækdal, Safety and pharmacokinetics of single and multiple ascending doses of the novel oral human GLP-1 analogue, oral semaglutide, in healthy subjects and subjects with type 2 diabetes, Clin. Pharmacokinet. 58 (2019) 781–791.
[12] S.T. Buckley, T.A. Bækdal, A. Vegge, S.J. Maarbjerg, C. Pyke, J. Ahnfelt-Rønne, K. G. Madsen, S.G. Schéele, T. Alanentalo, R.K. Kirk, B.L. Pedersen, R.B. Skyggebjerg, A.J. Benie, H.M. Strauss, P.-O. Wahlund, S. Bjerregaard, E. Farkas, C. Fekete, F. L. Søndergaard, J. Borregaard, M.-L. Hartoft-Nielsen, L.B. Knudsen, Transcellular stomach absorption of a derivatized glucagon-like peptide-1 receptor agonist, Sci. Transl. Med. 10 (2018) eaar7047.
[13] D.J. Brayden, S. Maher, Transient permeation enhancer® (TPE®) technology for oral delivery of octreotide: a technological evaluation, Expert Opin. Drug Deliv. 18 (2021) 1501–1512.
[14] S. Fattah, M. Ismaiel, B. Murphy, A. Rulikowska, J.M. Frias, D.C. Winter, D. J. Brayden, Salcaprozate sodium (SNAC) enhances permeability of octreotide across isolated rat and human intestinal epithelial mucosae in Ussing chambers, Eur. J. Pharm. Sci. 154 (2020) 105509.
[15] S. Maher, D.J. Brayden, Formulation strategies to improve the efficacy of intestinal permeation enhancers, Adv. Drug Deliv. Rev. 177 (2021) 113925.
[16] S. Maher, R.J. Mrsny, D.J. Brayden, Intestinal permeation enhancers for oral peptide delivery, Adv. Drug Deliv. Rev. 106 (Pt B) (2016) 277–319.
[17] Y. Yuts, M. Bohley, A. Krivitsky, Y. Bao, Z. Luo, J.-C. Leroux, Photopolymerization inks for 3D printing of elastic, strong, and biodegradable oral delivery devices, Adv. Funct. Mater. 34 (2024) 2310111.
[18] K. Whitehead, Z. Shen, S. Mitragotri, Oral delivery of macromolecules using intestinal patches: applications for insulin delivery, J. Control. Release 98 (2004) 37–45.
[19] G. Arrick, D. Sticker, A. Ghazal, Y. Lu, T. Duncombe, D. Gwynne, B. Mouridsen, J. Wainer, J.P.H. Jepsen, T.S. Last, D. Schultz, K. Hess, E. Medina De Alba, S. Min, M. Poulsen, C. Anker, P. Karandikar, H.D. Pedersen, J. Collins, N.E. Egecioglu, S. Tamang, C. Cleveland, K. Ishida, A.H. Uhrenfeldt, J. Kuosmanen, M. Pereverzina, A. Hayward, R.K. Kirk, S. You, C.M. Dalsgaard, S.B. Gunnarsson, I. Patsi, A. Bohr, A. Azzarello, M.R. Frederiksen, P. Herskind, J. Li, N. Roxhed, U.L. Rahbek, J. J. Water, S.T. Buckley, G. Traverso, Cephalopod-inspired jetting devices for gastrointestinal drug delivery, Nature 636 (2024) 481–487.
[20] A.K. Dhalla, Z. Al-Shamsie, S. Beraki, A. Dasari, L.C. Fung, L. Fusaro, A. Garapaty, B. Gutierrez, D. Gratta, M. Hashim, K. Horlen, P. Karamchedu, R. Korupolu, E. Liang, C. Ong, Z. Owyang, V. Salgotra, S. Sharma, B. Syed, M. Syed, A.T. Vo, R. Abdul-Wahab, A. Wasi, A. Yamaguchi, S. Yen, M. Imran, A robotic pill for oral delivery of biotherapeutics: safety, tolerability, and performance in healthy subjects, Drug Deliv. Transl. Res. 12 (2022) 294–305.
[21] A. Abramson, E. Caffarel-Salvador, M. Khang, D. Dellal, D. Silverstein, Y. Gao, M. R. Frederiksen, A. Vegge, F. Hubálek, J.J. Water, A.V. Friderichsen, J. Fels, R. K. Kirk, C. Cleveland, J. Collins, S. Tamang, A. Hayward, T. Landh, S.T. Buckley, N. Roxhed, U. Rahbek, R. Langer, G. Traverso, An ingestible self-orienting system for oral delivery of macromolecules, Science 363 (2019) 611–615.
[22] A. Abramson, M.R. Frederiksen, A. Vegge, B. Jensen, M. Poulsen, B. Mouridsen, M. O. Jespersen, R.K. Kirk, J. Windum, F. Hubálek, J.J. Water, J. Fels, S. B. Gunnarsson, A. Bohr, E.M. Straarup, M.W.H. Ley, X. Lu, J. Wainer, J. Collins, S. Tamang, K. Ishida, A. Hayward, P. Herskind, S.T. Buckley, N. Roxhed, R. Langer, U. Rahbek, G. Traverso, Oral delivery of systemic monoclonal antibodies, peptides and small molecules using gastric auto-injectors, Nat. Biotechnol. 40 (2022) 103–109.
[23] G. Traverso, C.M. Schoellhammer, A. Schroeder, R. Maa, G.Y. Lauwers, B.E. Polat, D.G. Anderson, D. Blankschtein, R. Langer, Microneedles for drug delivery via the gastrointestinal tract, J. Pharm. Sci. 104 (2015) 362–367.
[24] X. Gao, J. Li, J. Li, M. Zhang, J. Xu, Pain-free oral delivery of biologic drugs using intestinal peristalsis–actuated microneedle robots, Sci. Adv. 10 (2024) eadj7067.

[25] A. Abramson, E. Caffarel-Salvador, V. Soares, D. Minahan, R.Y. Tian, X. Lu, D. Dellal, Y. Gao, S. Kim, J. Wainer, J. Collins, S. Tamang, A. Hayward, T. Yoshitake, H.-C. Lee, J. Fujimoto, J. Fels, M.R. Frederiksen, U. Rahbek, N. Roxhed, R. Langer, G. Traverso, A luminal unfolding microneedle injector for oral delivery of macromolecules, Nat. Med. 25 (2019) 1512–1518.

[26] S.P. Newman, Drug delivery to the lungs: challenges and opportunities, Ther. Deliv. 8 (2017) 647–661.

[27] J.O. Morales, K.R. Fathe, A. Brunaugh, S. Ferrati, S. Li, M. Montenegro-Nicolini, Z. Mousavikhamene, J.T. McConville, M.R. Prausnitz, H.D.C. Smyth, Challenges and future prospects for the delivery of biologics: oral mucosal, pulmonary, and transdermal routes, AAPS J. 19 (2017) 652–668.

[28] M.I. Ugwoke, N. Verbeke, R. Kinget, The biopharmaceutical aspects of nasal mucoadhesive drug delivery, J. Pharm. Pharmacol. 53 (2001) 3–21.

[29] H.R. Costantino, L. Illum, G. Brandt, P.H. Johnson, S.C. Quay, Intranasal delivery: physicochemical and therapeutic aspects, Int. J. Pharm. 337 (2007) 1–24.

[30] Y. Zhang, J. Yu, A.R. Kahkoska, J. Wang, J.B. Buse, Z. Gu, Advances in transdermal insulin delivery, Adv. Drug Deliv. Rev. 139 (2019) 51–70.

[31] A.H. de Boer, The environmental burden of inhalation, Eur. J. Pharm. Sci. 204 (2025) 106893.

[32] A.H. Shojaei, Buccal mucosa as a route for systemic drug delivery: a review, J. Pharm. Pharm. Sci. 1 (1998) 15–30.

[33] V. Hearnden, V. Sankar, K. Hull, D.V. Juras, M. Greenberg, A.R. Kerr, P. B. Lockhart, L.L. Patton, S. Porter, M.H. Thornhill, New developments and opportunities in oral mucosal drug delivery for local and systemic disease, Adv. Drug Deliv. Rev. 64 (2012) 16–28.

[34] S. Şenel, A.A. Hıncal, Drug permeation enhancement via buccal route: possibilities and limitations, J. Control. Release 72 (2001) 133–144.

[35] V.F. Patel, F. Liu, M.B. Brown, Advances in oral transmucosal drug delivery, J. Control. Release 153 (2011) 106–116.

[36] H.P. Merkle, G. Wolany, Buccal delivery for peptide drugs, J. Control. Release 21 (1992) 155–164.

[37] I.A. Siegel, K.T. Izutsu, E. Watson, Mechanisms of non-electrolyte penetration across dog and rabbit oral mucosa in vitro, Arch. Oral Biol. 26 (1981) 357–361.

[38] J.O. Morales, S. Huang, R.O. Williams 3rd, J.T. McConville, Films loaded with insulin-coated nanoparticles (ICNP) as potential platforms for peptide buccal delivery, Colloids Surf. B: Biointerfaces 122 (2014) 38–45.

[39] Y. Xu, X. Zhang, Y. Zhang, J. Ye, H.-L. Wang, X. Xia, Y. Liu, Mechanisms of deformable nanovesicles based on insulin-phospholipid complex for enhancing buccal delivery of insulin, Int. J. Nanomedicine 13 (2018) 7319–7331.

[40] S. Bashyal, J.-E. Seo, T. Keum, G. Noh, S. Lamichhane, S. Lee, Development, characterization, and ex vivo assessment of elastic liposomes for enhancing the buccal delivery of insulin, Pharmaceutics 13 (2021) 565.

[41] A.J. Hoogstraate, J.C. Verhoef, A. Pijpers, L.A. van Leengoed, J.H. Verheijden, H. E. Junginger, H.E. Boddé, In vivo buccal delivery of the peptide drug buserelin with glycodeoxycholate as an absorption enhancer in pigs, Pharm. Res. 13 (1996) 1233–1237.

[42] D.J. Brayden, V. Stuettgen, Sodium glycodeoxycholate and sodium deoxycholate as epithelial permeation enhancers: in vitro and ex vivo intestinal and buccal bioassays, Eur. J. Pharm. Sci. 159 (2021) 105737.

[43] V.V. Nair, P. Cabrera, C. Ramírez-Lecaros, M.O. Jara, D.J. Brayden, J.O. Morales, Buccal delivery of small molecules and biologics: of mucoadhesive polymers, films, and nanoparticles – an update, Int. J. Pharm. 636 (2023) 122789.

[44] E. Caffarel-Salvador, S. Kim, V. Soares, R.Y. Tian, S.R. Stern, D. Minahan, R. Yona, X. Lu, F.R. Zakaria, J. Collins, J. Wainer, J. Wong, R. McManus, S. Tamang, S. McDonnell, K. Ishida, A. Hayward, X. Liu, F. Hubálek, J. Fels, A. Vegge, M. R. Frederiksen, U. Rahbek, T. Yoshitake, J. Fujimoto, N. Roxhed, R. Langer, G. Traverso, A microneedle platform for buccal macromolecule delivery, Sci. Adv. 7 (2021) eabe2620.

[45] Y. He, D. He, L. Fan, S. Ren, L. Wang, J. Sun, Application of hydrogel microneedles in the oral cavity, Biopolymers 115 (2024) e23573.

[46] K. Aran, M. Chooljian, J. Paredes, M. Rafi, K. Lee, A.Y. Kim, J. An, J.F. Yau, H. Chum, I. Conboy, N. Murthy, D. Liepmann, An oral microjet vaccination system elicits antibody production in rabbits, Sci. Transl. Med. 9 (2017) eaaf6413.

[47] S. Malhotra, T. Lijnse, E.O. Cearbhaill, D.J. Brayden, Devices to overcome the buccal mucosal barrier to administer therapeutic peptides, Adv. Drug Deliv. Rev. 220 (2025) 115572.

[48] Z. Luo, D. Klein Cerrejon, S. Römer, N. Zoratto, J.-C. Leroux, Boosting systemic absorption of peptides with a bioinspired buccal-stretching patch, Sci. Transl. Med. 15 (2023) eabq1887.

[49] D. Klein Cerrejon, H. Krupke, D. Gao, N. Paunović, D. Sachs, J.-C. Leroux, Optimized suction patch design for enhanced transbuccal macromolecular drug delivery, J. Control. Release 380 (2025) 875–891.

[50] A. Samir, F.H. Ashour, A.A.A. Hakim, M. Bassyouni, Recent advances in biodegradable polymers for sustainable applications, Npj Mater. Degrad. 6 (2022) 68.

[51] N. Paunović, J.-C. Leroux, Y. Bao, 3D printed elastomers with Sylgard-184-like mechanical properties and tuneable degradability, Polym. Chem. 13 (2022) 2271–2276.

[52] N. Paunović, Y. Bao, F.B. Coulter, K. Masania, A.K. Geks, K. Klein, A. Rafsanjani, J. Cadalbert, P.W. Kronen, N. Kleger, A. Karol, Z. Luo, F. Rüber, D. Brambilla, B. von Rechenberg, D. Franzen, A.R. Studart, J.-C. Leroux, Digital light 3D printing of customized bioresorbable airway stents with elastomeric properties, Sci. Adv. 7 (2021) eabe9499.

[53] J.J.E. Choi, J. Zwirner, R.S. Ramani, S. Ma, H.M. Hussaini, J.N. Waddell, N. Hammer, Mechanical properties of human oral mucosa tissues are site dependent: a combined biomechanical, histological and ultrastructural approach, Clin. Exp. Dent. Res. 6 (2020) 602–611.

[54] J.J.E. Choi, S. Chen, J.N. Waddell, Investigation of dental elastomers as oral mucosa simulant materials, Clin. Exp. Dent. Res. 7 (2021) 754–762.

[55] Pavel Iakubovskii, Segmentation Models Library, GitHub. https://github.com/qubvel/segmentation_models, 2019.

[56] Benoit Dehapiot, ETH-ScopeM_Krupke, GitHub. https://github.com/BDehapiot/ETH-ScopeM_Krupke, 2024 (accessed March 13, 2025).

[57] C.A. Schneider, W.S. Rasband, K.W. Eliceiri, NIH Image to ImageJ: 25 years of image analysis, Nat. Methods 9 (2012) 671–675.

[58] Artem Taturevych, csv-import-points, GitHub. https://github.com/xarial/codestack/commits/master/solidworks-api/document/sketch/csv-import-points, 2020 (accessed January 21, 2025).

[59] Y. Zhang, M. Huo, J. Zhou, S. Xie, PKSolver: An add-in program for pharmacokinetic and pharmacodynamic data analysis in Microsoft Excel, Comput. Methods Prog. Biomed. 99 (2010) 306–314.

[60] D.G. Johns, L.-C. Campeau, P. Banka, A. Bautmans, T. Bueters, E. Bianchi, D. Branca, P.G. Bulger, I. Crevecoeur, F.-X. Ding, R.M. Garbaccio, E.D. Guetschow, Y. Guo, S.N. Ha, J.M. Johnston, H. Josien, E.A. Kauh, K.A. Koeplinger, J.T. Kuethe, E. Lai, C.L. Lanning, A.Y.H. Lee, L. Li, A.G. Nair, E.A. O'Neill, S.A. Stoch, D. A. Thaisrivongs, T.J. Tucker, P. Vachal, K. van Dyck, F.P. Vanhoutte, B. Volckaert, D.G. Wolford, A. Xu, T. Zhao, D. Zhou, S. Zhou, X. Zhu, H.J. Zokian, A.M. Walji, H. B. Wood, Orally bioavailable macrocyclic peptide that inhibits binding of PCSK9 to the low density lipoprotein receptor, Circulation 148 (2023) 144–158.

[61] M. Wolff, I. Kleinberg, Oral mucosal wetness in hypo- and normosalivators, Arch. Oral Biol. 43 (1998) 455–462.

[62] K. Shima, Y. Tamura, T. Tsuji, A. Kandori, M. Yokoe, S. Sakoda, Estimation of human finger tapping forces based on a fingerpad-stiffness model, Annu. Int. Conf. IEEE Eng. Med. Biol. Soc. IEEE (2009) 2663–2667.

[63] S. Dhillon, S.J. Keam, Bremelanotide: first approval, Drugs 79 (2019) 1599–1606.

[64] E. Chiellini, A. Corti, S. D'Antone, R. Solaro, Biodegradation of poly(vinyl alcohol) based materials, Prog. Polym. Sci. 28 (2003) 963–1014.

[65] US Food and Drug Administration (FDA), Multidiscipline Review NDA 210557 Vyleesi. https://www.accessdata.fda.gov/drugsatfda_docs/nda/2019/210557Orig1s000MultidisciplineR.pdf, 2019 (accessed March 3, 2025).

[66] S. Schmidt, C. Scherkus, J. Muschiol, U. Menyes, T. Winkler, W. Hummel, H. Gröger, A. Liese, H.-G. Herz, U.T. Bornscheuer, An enzyme cascade synthesis of ε-caprolactone and its oligomers, Angew. Chem. Int. Ed. 54 (2015) 2784–2787.

[67] B. Wu, X. Feng, W. Du, Z. Li, G. Qian, X. Duan, X. Zhou, Z. Liu, J. Zhang, Continuous synthesis of ε-caprolactone in a microreactor and kinetics insights into its side reactions, J. Flow Chem. 14 (2024) 337–347.

[68] B.G. Amsden, G. Misra, F. Gu, H.M. Younes, Synthesis and characterization of a photo-cross-linked biodegradable elastomer, Biomacromolecules 5 (2004) 2479–2486.

[69] S. Kaihara, S. Matsumura, A.G. Mikos, J.P. Fisher, Synthesis of poly(L-lactide) and polyglycolide by ring-opening polymerization, Nat. Protoc. 2 (2007) 2767–2771.

[70] A. Hermann, S. Hill, A. Metz, J. Heck, A. Hoffmann, L. Hartmann, S. Herres-Pawlis, Next generation of zinc bisguanidine polymerization catalysts towards highly crystalline, biodegradable polyesters, Angew. Chem. Int. Ed. 59 (2020) 21778–21784.

[71] U. Herber, K. Hegner, D. Wolters, R. Siris, K. Wrobel, A. Hoffmann, C. Lochenie, B. Weber, D. Kuckling, S. Herres-Pawlis, Iron(II) and zinc(II) complexes with tetradentate bis(pyrazolyl)methane ligands as catalysts for the ring-opening polymerisation of *rac*-lactide, Eur. J. Inorg. Chem. 2017 (2017) 1341–1354.

[72] F.P. Byrne, S. Jin, G. Paggiola, T.H.M. Petchey, J.H. Clark, T.J. Farmer, A.J. Hunt, C.R. McElroy, J. Sherwood, Tools and techniques for solvent selection: green solvent selection guides, Sustain. Chem. Process. 4 (2016) 7, in: https://sustainablechemicalprocesses.springeropen.com/articles/10.1186/s40508-016-0051-z.

[73] A.I. Cooper, Polymer synthesis and processing using supercritical carbon dioxide, J. Mater. Chem. 10 (2000) 207–234.

[74] V.S. Kaplin, N.N. Glagolev, V.T. Shashkova, I.A. Matveeva, I.V. Shershnev, T. S. Zarkhina, N.V. Minaev, N.A. Aksenova, B.S. Shavkuta, E.A. Bezrukov, A. S. Kopylov, D.S. Kuznetsova, A.I. Shpichka, P.S. Timashev, A.B. Solovieva, Photocurable methacrylate derivatives of polylactide: a two-stage synthesis in supercritical carbon dioxide and 3D laser structuring, Polymers 12 (2020) 2525.

[75] Y. Wang, G.A. Ameer, B.J. Sheppard, R. Langer, A tough biodegradable elastomer, Nat. Biotechnol. 20 (2002) 602–606.

Update

Journal of Controlled Release

Volume 388, Issue P1, 10 December 2025, Page

DOI: https://doi.org/10.1016/j.jconrel.2025.114270

Journal of Controlled Release 388 (2025) 114270

Contents lists available at ScienceDirect

Journal of Controlled Release

journal homepage: www.elsevier.com/locate/jconrel

Corrigendum

Corrigendum to 'A biodegradable suction patch for sustainable transbuccal peptide delivery' [J Control Release. 384 (2025) 113947]

Hanna Krupke [a], Nicole Zoratto [a], Lucie Rabut [a], Daniel Gao [a], Nevena Paunović [a], David Klein Cerrejon [a], Benoit Dehapiot [b], Jean-Christophe Leroux [a,*]

[a] Institute of Pharmaceutical Sciences, Department of Chemistry and Applied Biosciences, ETH Zurich, 8093 Zurich, Switzerland
[b] Scientific Center for Optical and Electron Microscopy (ScopeM), ETH Zurich, 8093 Zurich, Switzerland

The authors regret a typo in Section 2.15. "Cryosectioning, staining, and imaging of *ex vivo* samples". This section contained errors referring to the concentrations of phalloidin-iFluor 488 reagent and Hoechst.

The sentence: "Then, samples were stained by incubation for 30 min in 1% (v/v) phalloidin-iFluor 488 reagent and 1% (v/v) Hoechst in 1% (m/v) BSA solution in PBS, followed by washing in PBS for 3 min and mounting with ProLong™ Diamond Antifade Mountant."

Should read as follows: "Then, samples were stained by incubation for 30 min in 0.1% (v/v) phalloidin-iFluor 488 reagent and 0.1% (v/v) Hoechst in 1% (m/v) BSA solution in PBS, followed by washing in PBS for 3 min and mounting with ProLong™ Diamond Antifade Mountant."

The overall results and findings of the article are not impacted by this correction.

The authors would like to apologise for any inconvenience caused.

DOI of original article: https://doi.org/10.1016/j.jconrel.2025.113947

* Corresponding author.
E-mail address: jleroux@ethz.ch (J.-C. Leroux).

https://doi.org/10.1016/j.jconrel.2025.114270

Available online 1 October 2025